

Network Cosmology

Dmitri Krioukov,¹ Maksim Kitsak,¹ Robert S. Sinkovits,² David Rideout,³ David Meyer,³ and Marián Boguñá⁴

¹Cooperative Association for Internet Data Analysis (CAIDA),

University of California, San Diego (UCSD), La Jolla, CA 92093, USA

²San Diego Supercomputer Center (SDSC), University of California, San Diego (UCSD), La Jolla, CA 92093, USA

³Department of Mathematics, University of California, San Diego (UCSD), La Jolla, CA 92093, USA

⁴Departament de Física Fonamental, Universitat de Barcelona, Martí i Franquès 1, 08028 Barcelona, Spain

Causal sets are an approach to quantum gravity in which the causal structure of spacetime plays a fundamental role. The causal set is a quantum network which underlies the fabric of spacetime. The nodes in this network are tiny quanta of spacetime, with two such quanta connected if they are causally related. Here we show that the structure of these networks in de Sitter spacetime, such as our accelerating universe, is remarkably similar to the structure of complex networks—the brain or the Internet, for example. Specifically, we show that the node degree distribution of causal sets in de Sitter spacetime is described by a power law with exponent 2, similar to many complex networks. Quantifying the differences between the causal set structure in de Sitter spacetime and in the real universe, we find that since the universe today is relatively young, its power-law exponent is not 2 but 3/4, yet exponent 2 is currently emerging. Finally, we show that as a consequence of a simple geometric duality, the growth dynamics of complex networks and de Sitter causal sets are asymptotically identical. These findings suggest that unexpectedly similar mechanisms may shape the large-scale structure and dynamics of complex systems as different as the brain, the Internet, and the universe.

The finite speed of light c is a fundamental constant of our physical world, responsible for the non-trivial causal structure of the universe [1]. If in some coordinate system the spatial distance x between two spacetime events (points in space and time) is larger than ct , where t is the time difference between them, then these two events cannot be causally related since no signal can propagate faster than c (Fig. 1(a)). Causality is fundamental not only in physics, but also in fields as disparate as distributed systems [2, 3], criminology [4], and philosophy [5].

Causal sets [6] are the main building block in an approach to quantum gravity, motivated by mathematical results stating that the structure of a relativistic spacetime is almost fully determined by its causal structure alone [7–9], suggesting that this structure is fundamental. At a fundamentally tiniest scale (the Planck scale, $l_P \sim 10^{-35}$ meters and $t_P \sim 10^{-43}$ seconds), one expects spacetime not to be continuous but to have a discrete structure [10], similar to ordinary matter, which is not continuous at atomic scales but instead is composed of discrete atoms. The causal set approach postulates that spacetime at the Planck scale is a discrete causal set, or *causet*. A causet is a set of elements (Planck-scale “atoms” of spacetime) endowed with causal relationships among them. A causet is thus a network in which nodes are spacetime quanta, and links are causal relationships between them. To make contact with General Relativity, one expects the theory to give rise to causal sets which are constructed by a Poisson process, i.e.

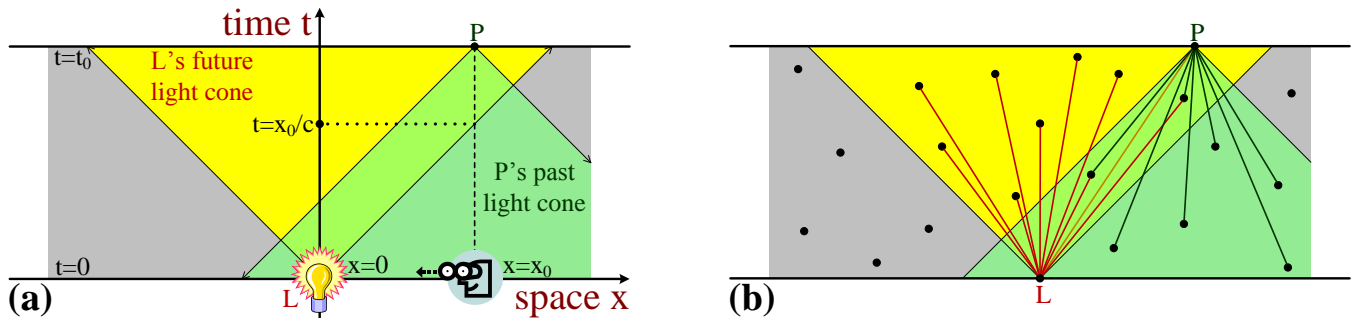


FIG. 1: Finite speed of light c , and causal structure of spacetime. In panel (a), a light source located at spatial coordinate $x = 0$ is switched on at time $t = 0$. This event, denoted by L in the figure, is not immediately visible to an observer located at distance x_0 from the light source. The observer does not see any light until time $t = x_0/c$. Since no signal can propagate faster than c , the events on the observer’s world line, shown by the vertical dashed line, are not causally related to L until the world line enters the L ’s future light cone (yellow color) at $t = x_0/c$. This light cone depicts the set of events that L can causally influence. An example is event P located on the observer’s world line $x = x_0$ at time $t = t_0 > x_0/c$. The past light cone of P (green color) is the set of events that can causally influence P . Events L and P lie within each other’s light cones. Panel (b) shows a set of points sprinkled into the considered spacetime patch. The red and green links show all causal connections of events L and P in the resulting causet. These links form a subset of all the links in the causet (not shown).

by sprinkling points into spacetime uniformly at random, and then connecting each pair of points iff they lie within each other's light cones (Fig. 1(b)). According to the theorem in [11], causets constructed by Poisson sprinkling are relativistically invariant, as opposed to regular lattices, for example. Therefore we will use Poisson sprinkling here to construct causets corresponding to spacetimes. One of the goals in the causal set approach to quantum gravity, which we discuss no further here, is to identify causet growth laws based on fundamental physical principles which can grow causets similar to those obtained by Poisson sprinkling onto the spacetime of our universe [12, 13].

In 1998 the expansion of our universe was found to be accelerating [14, 15]. Positive vacuum energy, or *dark energy*, corresponding to a positive cosmological constant Λ in the Einstein equations (Section II), is currently the most plausible explanation for this acceleration. Positive Λ implies that the universe is asymptotically (at late times) described by de Sitter spacetime [16, 17]. We first consider the structure of causets sprinkled onto de Sitter spacetime, and then quantify how different this structure is in the real universe.

De Sitter spacetime is the solution of Einstein's field equations for an empty universe with positive Λ . The 1 + 1-dimensional de Sitter spacetime (the first '1' stands for the space dimension; the second '1'—for time) can be visualized as a one-sheeted 2-dimensional hyperboloid embedded in a flat 3-dimensional Minkowski space (Fig. 2(a)). The length of horizontal circles in Fig. 2(a), corresponding to the volume of space at a moment of time, grows exponentially with time t . Since causet nodes are distributed uniformly over spacetime, their number also grows exponentially with time. Specifically, the number of nodes in a patch of $d + 1$ -dimensional de Sitter spacetime between $t = 0$ and $t = t_0$ (the "current" time) scales as $e^{d(t-t_0)/a}$, where $a = \sqrt{3/\Lambda}$ is the inverse square root of the spacetime curvature (Section II). A node born at time t is connected to all nodes lying within its future light cone up to current time t_0 . Since the node density is uniform, the expected number of such nodes and consequently the number of future connections emanating from the node born at time t are proportional to the volume of this light cone, which scales as $e^{d(t_0-t)/a}$ (Section II). We thus have a combination of two exponentials, number of nodes $\sim e^{\alpha t}$ born at time t and their degrees $\sim e^{-\beta t}$, where $\alpha = \beta = d/a$. This combination yields a power-law distribution $P(k) \sim k^{-\gamma}$ of node degrees k in the causet, where exponent $\gamma = \alpha/\beta + 1 = 2$.

In many complex networks the degree distribution is also a power law with γ close to 2 [19, 20]. In Fig. 3 we show two examples, the brain and the Internet, and juxtapose them against a de Sitter causet. In all the three networks, the exponent $\gamma \approx 2$.

Is there a connection revealing a *mechanism* responsible for the emergence of this structural similarity, going beyond the degree distribution, and showing that other structural and dynamical properties of complex networks and de Sitter causets are similar? Remarkably, the answer is yes. To see this, consider a new spacetime quantum P that has just been born at current time $t = t_0$ in Fig. 2. Upon its birth, P causally connects to all nodes in its past light cone. As illustrated in Fig. 2, we map this past light cone to the upper sheet of the dual two-sheeted inner hyperboloid, which is the standard hyperboloid representation of the hyperbolic plane [23]. This mapping sends P 's past light cone in the de Sitter spacetime to a hyperbolic disc of radius t_0 centered at P 's image in the hyperbolic space. Therefore upon this mapping, the causal network becomes asymptotically identical to the complex networks in the model [18] shown to accurately describe the large-scale structure and growth dynamics of some complex networks, such as the Internet, metabolic networks, etc. Indeed, in that model, angular (spatial) distances in the hyperbolic space abstract intrinsic similarity distances between nodes in the network, while the radial (time) coordinate of a node is a function of its birth time. According to the model, new node P is born at a random location on the edge of an expanding hyperbolic disc of radius r_0 , and connects to all existing nodes that lie within the hyperbolic disc of the same radius r_0 but centered at P . If we identify $r_0 \equiv t_0$, then this disc is asymptotically identical to P 's past light cone (Fig. 2). All further details are given in Section II, where we show that the de Sitter causet is a particular case of [18] with $\gamma = 2$ and strongest possible clustering, i.e. with the largest possible number of triangular subgraphs. Strong clustering is another structural property often observed in complex networks [19, 20]. Considering causet growth as the birth of new nodes as the current time boundary $t = t_0$ moves forward one causet element at a time, we conclude that the established equivalence implies that not only the structure, but also the growth dynamics of complex networks and de Sitter causets are asymptotically identical.

The real universe is only *asymptotically* de Sitter [16, 17]. Due to non-zero matter density, the spacetime structure of the universe deviates from the structure of de Sitter spacetime. In fact, the matter and dark energy densities are of the same order of magnitude in the universe now, a coincidence known as a "why now?" puzzle in cosmology [24–26]. This coincidence implies that the current rescaled cosmological time $\tau_0 = t_0/a$ is approximately 1, meaning that the universe is relatively young today. It transitions from the past matter-dominated era ($\tau < 1$) to the future dark-energy-dominated era ($\tau > 1$). Since universe evolution has been dominated not by dark energy, but by matter, the degree distribution in the universe causet is a power law with exponent $\gamma = 3/4$, instead of $\gamma = 2$ (Fig. 4(a)). Yet, since dark energy begins to dominate, the $\gamma = 2$ scaling is currently emerging. Figure 4(b) traces the evolution of the degree distribution in the universe in its past and future. According to the figure, in the matter-dominated era with $\tau < 1$, the degree distribution is a power law with exponent $3/4$ up to a soft cut-off that grows with time. Above this soft cut-off, the distribution decays sharply. Once we reach times $\tau \sim 1$, e.g. today, we enter the dark-

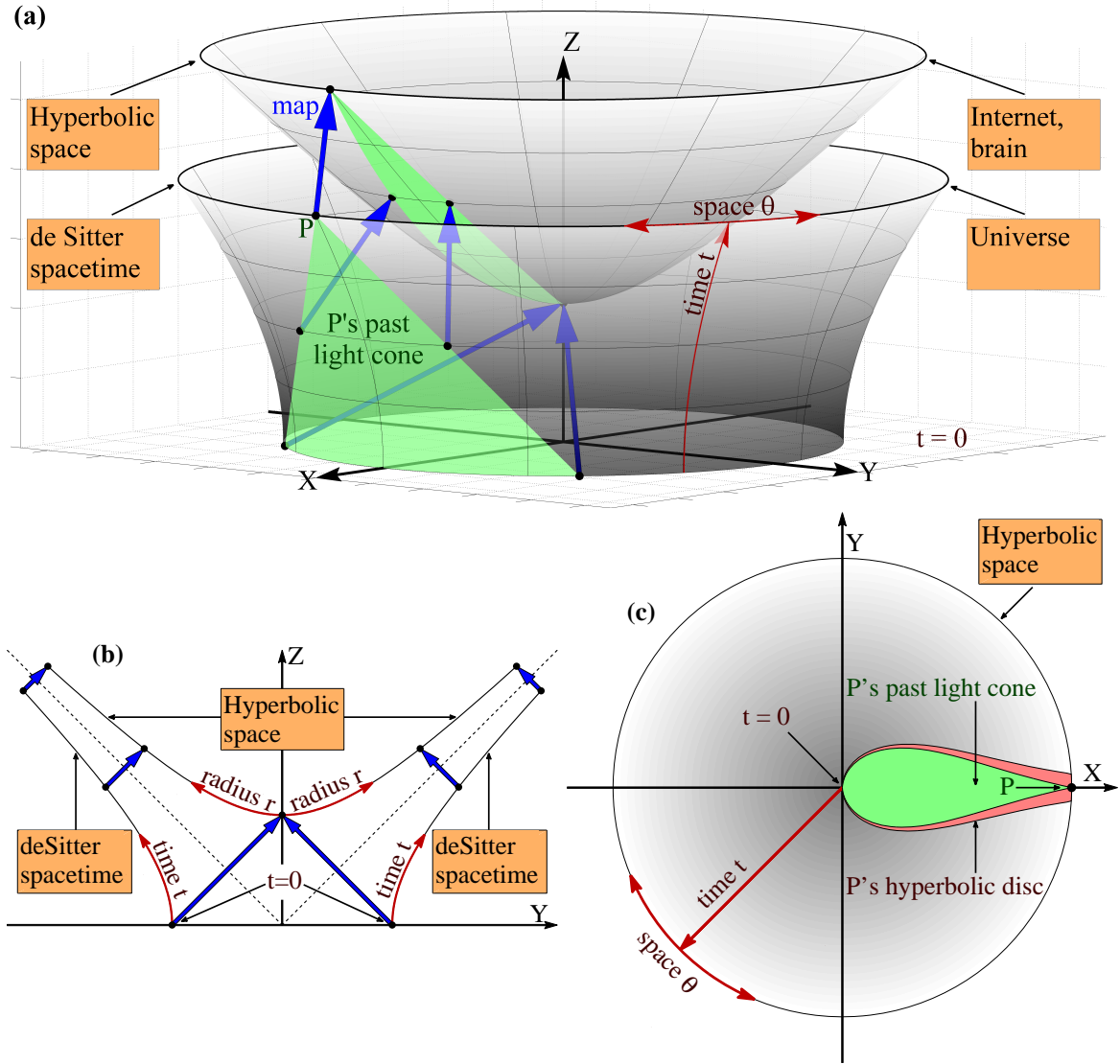


FIG. 2: Mapping between the de Sitter universe and complex networks. Panel (a) shows the 1 + 1-dimensional de Sitter spacetime represented by the upper half of the outer one-sheeted hyperboloid in the 3-dimensional Minkowski space XYZ . The spacetime coordinates (θ, t) , shown by the red arrows, cover the whole de Sitter space. The spatial coordinate θ of any spacetime event, e.g. point P , is its polar angle, while its time t is the length of the arc connecting the point to the XY plane where $t = 0$. At any time t , the spatial slice of the spacetime is a circle. This 1-dimensional space expands exponentially with time. Dual to the outer hyperboloid is the inner hyperboloid—the hyperbolic 2-dimensional space, i.e. the hyperbolic plane, represented by the upper sheet of a two-sheeted hyperboloid. The mapping between the two hyperboloids is shown by the blue arrows. The green shapes show the past light cone of point P in the Sitter space, and the projection of this light cone onto the hyperbolic plane under the mapping. Point P is causally connected to all the spacetime quanta lying within its green shape. Panel (b) depicts the cut of panel (a) by the YZ plane to further illustrate the mapping, shown also by the blue arrows. The mapping is just the reflection between the two hyperboloids with respect to the cone shown by the dashed lines. Panel (c) projects the inner hyperboloid (the hyperbolic plane) with the P 's past light cone (the green shape) onto the XY plane. The red shape is the left half of the hyperbolic disc centered at P and having the radius equal to P 's time t , which in this representation is P 's radial coordinate, i.e. the distance between P and the origin of the XY plane. In the hyperbolic model of complex networks [18], a new node P connects to all the existing nodes lying within this red shape. The green and red shapes become indistinguishable at large times t , establishing the equivalence between the causal structure of the de Sitter universe, and the large-scale structure of complex networks.

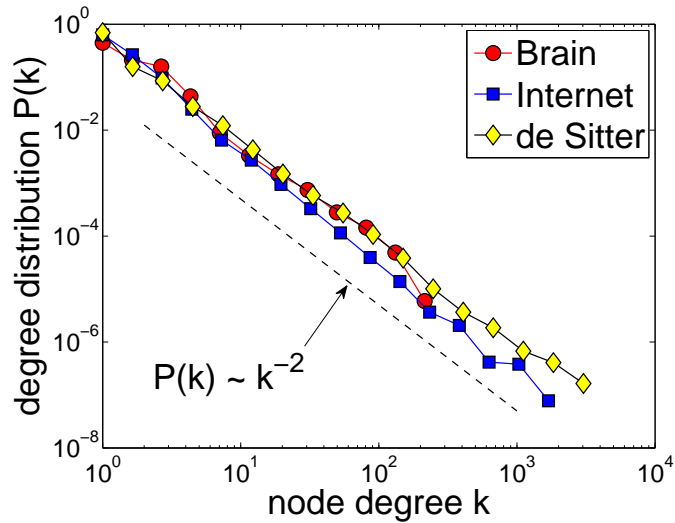


FIG. 3: Degree distributions in the brain, Internet, and de Sitter spacetime. The degree distribution $P(k)$ is the number of nodes $N(k)$ of degree k divided by the total number of nodes N in the networks, $P(k) = N(k)/N$. The *brain* is a functional network of the human brain obtained from the fMRI measurements in [21]. The *Internet* is the network representing economic relations between autonomous systems, extracted from CAIDA's Internet topology measurements [22]. *De Sitter* is a causal set in the 1 + 1-dimensional de Sitter spacetime. The sizes of the three networks are, respectively, 23713, 23752, and 23739, and their average node degrees are 6.14, 4.92, and 5.65. All further details are in Section I.

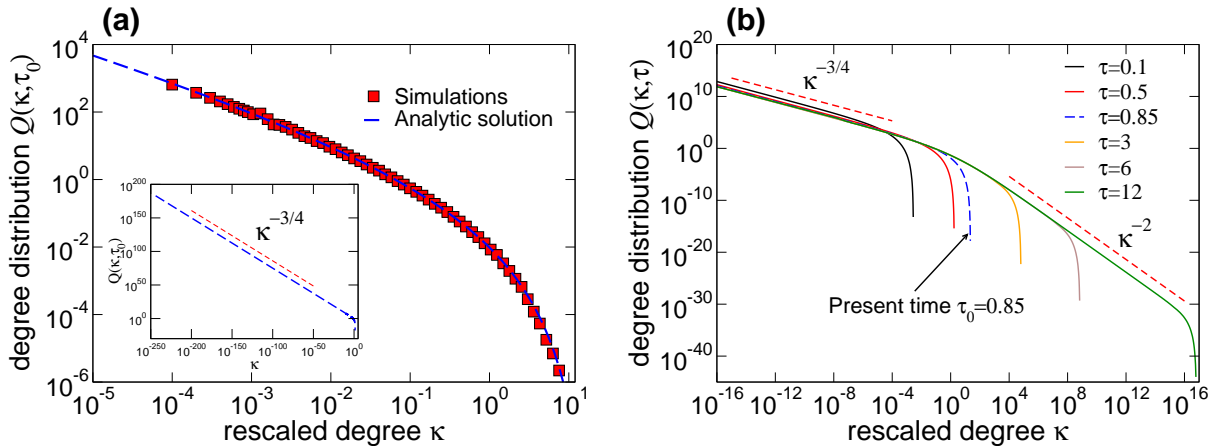


FIG. 4: Degree distribution in the universe. Panel (a) shows the rescaled distribution $Q(\kappa, \tau_0) = \delta a^4 P(k, t_0)$ of rescaled degrees $\kappa = k/(\delta a^4)$ in the universe causet at present time $\tau_0 = t_0/a = 0.85$, where δ is the constant node density in spacetime, and $a = \sqrt{3/\Lambda}$. As shown in Section III, the rescaled degree distribution does not depend on either δ or a , so we set them to $\delta = 10^4$ and $a = 1$ for convenience. The size N of simulated causets can be also set to any value without affecting the degree distribution, and this value is $N = 10^6$ nodes in the figure. The degree distribution in this simulated causet is juxtaposed against the numeric evaluation of the analytical solution for $Q(\kappa, \tau_0)$ shown by the blue dashed line. The inset shows this analytic solution for the whole range of node degrees $k \in [1, 10^{244}]$ in the universe, where $\delta \sim 10^{173}$ and $a \sim 5 \times 10^{17}$. Panel (b) shows the same solution for different values of rescaled time τ , tracing the evolution of the degree distribution in the universe. All further details are in Section III.

energy-dominated era. The part of the distribution with exponent $3/4$ freezes, while the soft cut-off transforms into a crossover to another power law with exponent 2, whose cut-off grows exponentially with time. The crossover point is located at $k_{cr} \sim \delta a^4$, where $\delta \equiv 1/(l_P^3 t_P)$ is the density of spacetime quanta. Nodes of small degrees $k < k_{cr}$ obey the $\gamma = 3/4$ part of the distribution, while high-degree nodes, $k > k_{cr}$, lie in its $\gamma = 2$ regime. At the future infinity $\tau \rightarrow \infty$, the distribution becomes a perfect double power law with exponents $3/4$ and 2. The detailed analysis of these statements and their proofs can be found in Section III.

In summary, the asymptotic causal structure of the de Sitter universe is unexpectedly similar to the large-scale structure of many complex networks. As the universe expands into the future, its causal set grows and the dynamics of this growth is asymptotically the same as the dynamics governing the large-scale evolution of the Internet and other networks. Geometrically, this equivalence is due to a simple duality between the two hyperboloids in Fig. 2. The inner hyperboloid represents the geometry of complex networks; the outer hyperboloid is the de Sitter spacetime, which is the solution to Einstein's equations for a universe with positive vacuum energy. In that sense, the Einstein equations provide an adequate description for the evolution of the Internet and other complex networks. Collectively these findings suggest that unexpectedly similar mechanisms whose precise nature and common origin remain to be identified, may shape the large-scale structure and dynamics of complex systems as different as the brain, the Internet, and the universe.

I. DATA AND SIMULATIONS

In this section we describe the data and methods used in Figs. 3&4. We note that in all the three considered networks, links represent soft relational data instead of hard-wired network diagrams: causal/correlation relations in the brain, economic/business relations in the Internet, and causal relations in causal sets.

A. Brain data

The brain functional network in Fig. 3 represents causal/correlation relations between small areas in the human brain. This network is extracted from the fMRI measurements in [21]. In those experiments, the whole brains of different human subjects are split into $36 \times 64 \times 64 = 147456$ adjacent areas called *voxels*, each voxel of volume $3 \times 3.475 \times 3.475 \text{ mm}^3$. The subjects are then asked to perform different tasks, during which the magnetic resonance activity $V(x, t)$ is recorded at each voxel x at time t . Time t is discrete: 400 recordings are made with the interval of 2.5 s. Given this data, and denoting by $\langle \cdot \rangle$ the time average, the correlation coefficient $r(x, x')$ for each pair of voxels is then computed:

$$r(x, x') = \frac{\langle V(x, t)V(x', t) \rangle - \langle V(x, t) \rangle \langle V(x', t) \rangle}{\sqrt{[\langle V(x, t)^2 \rangle - \langle V(x, t) \rangle^2][\langle V(x', t)^2 \rangle - \langle V(x', t) \rangle^2]}}. \quad (1)$$

To form a functional network out of this correlation data, two voxels x and x' are considered causally connected if the correlation coefficient between them exceeds a certain threshold r_c , $r(x, x') > r_c$. If r_c is too small or too large, then the resulting network is fully connected or fully disconnected. There exists however a unique percolation transition value of r_c corresponding to the onset of the giant component in the network. To find this value, we compute the sizes $|S_1|_{r_c}$ and $|S_2|_{r_c}$ of the largest and second largest components S_1 and S_2 in the network for different values of r_c . The value of threshold r_c corresponding to the largest values of $|\partial|S_1|/\partial r_c|_{r_c}$ and $|S_2|_{r_c}$ is then its percolation transition value. With threshold r_c set to this value, the network has a power-law degree distribution with exponent $\gamma = 2$ and exponential cutoffs, and this result is stable across different human subjects and different types of activity that they perform during measurements, see [21, 27] and http://www.caida.org/publications/papers/2012/network_cosmology/supplemental/. In Fig. 3, a specific dataset is used—*Set14*, see the URL—where the subject is at rest. The threshold value is $r_c = 0.7$.

B. Internet data

The Internet topology in Fig. 3 represent economic/business relations between *autonomous systems* or *ASs*. The AS is an organization or an individual owning a part of the Internet infrastructure. The network is extracted from the data collected by CAIDA's Archipelago Measurement Infrastructure (Ark) [22], <http://www.caida.org/projects/ark/>. The Ark infrastructure consists of a set of monitors continuously tracing IP-level paths to random destinations in the Internet. The union of the paths collected by all the monitors is then aggregated over a certain period of time, and each IP address in the collection is mapped to an AS owning this address, using the RouteViews BGP tables <http://www.routeviews.org/>. The resulting AS network has a power-law degree distribution with exponent $\gamma = 2.1$, and this result is stable over time [28, 29] and across different measurement methodologies [30, 31], <http://www.caida.org/publications/papers/2012/topocompare-tr/>. The data and its further description are available at http://www.caida.org/data/active/ipv4_routed_topology_aslinks_dataset.xml. In Fig. 3, the data for June 2009 is used. The aggregation period is one month, and the number of monitors is 36.

C. De Sitter causet

The causet in Fig. 3 is generated by sprinkling a number of points over a patch in the 1 + 1-dimensional de Sitter spacetime, and connecting each pair of points if they lie within the other's light cones. The point density is uniform in the de Sitter metric, and the size of the patch is such that the size of the generated causet and its average degree are close to those of the brain and the Internet.

In conformal time coordinates, see Section II A below, each spacetime point has two coordinates, spatial $\theta \in [0, 2\pi]$ and temporal $\eta \in (-\pi/2, \pi/2)$, with $\eta = -\pi/2$ and $\eta = \pi/2$ corresponding to the past and future infinities respectively. The spacetime patch that we consider is between $\eta = 0$ and $\eta = \eta_0 > 0$, where η_0 is determined below. This patch is illustrated in Fig. 2(a). To sample N points from this patch with uniform density, we sample N pairs of random

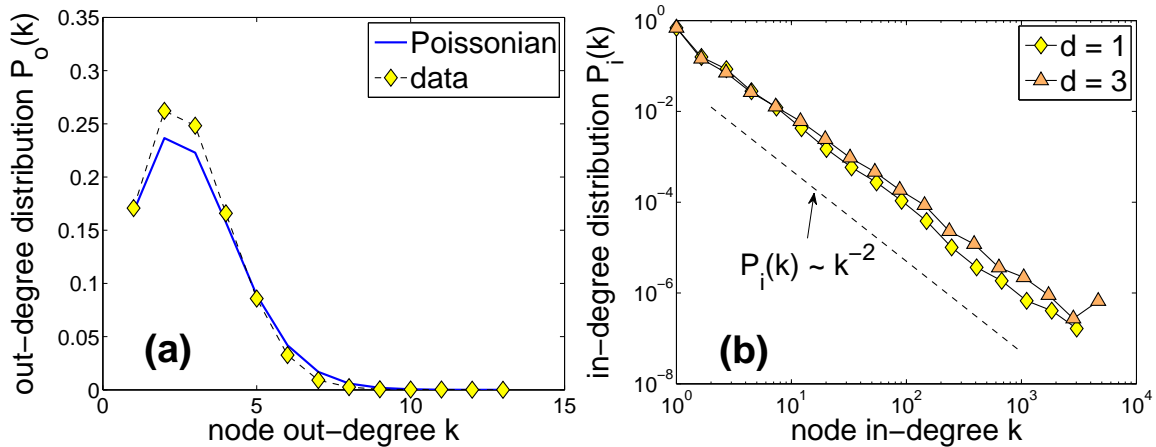


FIG. 5: (a) The out-degree distribution of the causet approximated by a patch of 1+1 dimensional de Sitter spacetime. The solid line shows the Poissonian distribution with the mean $\lambda = \bar{k}_o = \bar{k}/2 = 2.83$, where \bar{k}_o is the average out-degree in the causet. (b) The in-degree distribution of causets approximated by patches of 1+1 and 3+1 dimensional de Sitter spacetime. The causet sizes are $N = 23739$ and $N = 23732$, and their average degrees are $\bar{k} = 5.65$ and $\bar{k} = 5.25$ respectively.

numbers: N spatial coordinates θ drawn from the uniform distribution on $[0, 2\pi]$, and N temporal coordinates η drawn from the distribution

$$\rho(\eta|\eta_0) = \frac{\sec^2 \eta}{\tan \eta_0}. \quad (2)$$

Two spacetime points with coordinates (η, θ) and (η', θ') are then connected in the causet if $\Delta\theta < \Delta\eta$, where $\Delta\theta = \pi - |\pi - |\theta - \theta'||$ and $\Delta\eta = |\eta - \eta'|$ are the spatial and temporal distances between the points in this coordinate system.

To determine η_0 we first note that since the point density is uniform, the number of points N is proportional to the patch volume, and the proportionality coefficient is a constant point density δ . The volume of the patch is easy to calculate, see Section II A, where we can also calculate the average degree \bar{k} in the resulting causets, so that we have:

$$N = 2\pi\delta a^2 \tan \eta_0, \quad (3)$$

$$\bar{k} = 4\delta a^2 \left(\frac{\eta_0}{\tan \eta_0} + \ln \sec \eta_0 - 1 \right), \quad (4)$$

$$\frac{\bar{k}}{N} = \frac{2}{\pi} \cdot \frac{\eta_0 / \tan \eta_0 + \ln \sec \eta_0 - 1}{\tan \eta_0}, \quad (5)$$

where a is the spacetime's pseudoradius determining its curvature. Given a target average degree \bar{k} and number of nodes N in a causet, their ratio determines η_0 via the last equation. Sampling N points from this patch will then yield causets with expected average degree \bar{k} . The average degree in generated causets will not be exactly equal to \bar{k} since there will be nodes of degree 0 and Poissonian fluctuations of the numbers of nodes lying within light cones around their expected values. In Fig. 3, the exact number of sampled points is $N = 24586$ and target value of the average degree is $\bar{k} = 5.53$, so that the above equations yield $\eta_0 = \pi/2 - 3.86 \times 10^{-5}$ and $\delta a^2 = 0.151$. The resulting number of nodes excluding nodes of degree 0 and their average degree in the generated causet are reported in the caption of Fig. 3.

Figure 3 shows the in-degree distribution in the causet, with links oriented from the future to the past, i.e. from nodes with larger η to nodes with smaller η . The out-degree distribution is not particularly interesting, close to Poissonian, see Fig. 5(a).

In higher dimensions, pre-asymptotic effects become more prominent in causets of similar size and average degree. In particular, the exponent of the degree distribution is slightly below 2, see Fig. 5(b) comparing the causets in the $d = 1$ and $d = 3$ cases. The former causet is the same as in Fig. 3, while the latter is obtained by a procedure similar

to the one described above, except that instead of Eqs. (2-5), we have

$$\rho(\eta|\eta_0) = \frac{3 \sec^4 \eta}{(2 + \sec^2 \eta_0) \tan \eta_0}, \quad (6)$$

$$N = \frac{2}{3} \pi^2 \delta a^4 (2 + \sec^2 \eta_0) \tan \eta_0, \quad (7)$$

$$\bar{k} = \frac{4}{9} \pi \delta a^4 \frac{12(\eta_0/\tan \eta_0 + \ln \sec \eta_0) + (6 \ln \sec \eta_0 - 5) \sec^2 \eta_0 - 7}{2 + \sec^2 \eta_0}, \quad (8)$$

$$\frac{\bar{k}}{N} = \frac{2}{3\pi} \cdot \frac{12(\eta_0/\tan \eta_0 + \ln \sec \eta_0) + (6 \ln \sec \eta_0 - 5) \sec^2 \eta_0 - 7}{(2 + \sec^2 \eta_0)^2 \tan \eta_0}, \quad (9)$$

and each point has two additional angular coordinates, θ_1 and θ_2 , which are random variables between 0 and π drawn from distributions $(2/\pi) \sin^2 \theta_1$ and $(1/2) \sin \theta_2$, see Section II A. The spatial distance $\Delta\theta$ between pairs of points is then computed using the spherical law of cosines, and two points are causally linked if $\Delta\theta < \Delta\eta$ as before. In Fig. 5(b), the $d = 3$ causet has target $N = 25441$ and $\bar{k} = 5.29$, yielding $\eta_0 = \pi/2 - 4.11 \times 10^{-2}$ and $\delta a^4 = 0.267$. The maximum-likelihood fitting of the degree sequence in the $d = 3$ and $d = 1$ causets yields $\gamma = 1.65$ and $\gamma = 1.90$, while the least-square fitting of the complementary cumulative distribution function for node degrees yields $\gamma = 1.77$ and $\gamma = 1.98$.

D. Simulating the universe

The results in Section III below allow us to simulate the universe causet similarly to the de Sitter simulations described in the previous section. The main idea behind the universe simulations is that we can use the exact results for a flat universe, but apply them to a closed universe with an arbitrary finite number of nodes in its causet, since the real universe is almost flat, and since the degree distribution in both cases is the same.

Specifically, the causet in Fig. 4 is generated as follows. Unlike the previous section where only conformal time is used, here it is more convenient to begin with the rescaled time $\tau = t/a$. The current measurements of the universe yield, see Section III C, $\tau_0 = t_0/a = (2/3) \operatorname{arcsinh} \sqrt{\Omega_\Lambda/\Omega_M} = 0.8458$ as the best estimate for this rescaled time in the universe today. According to Eqs. (85,86), the scale factor is

$$R(\tau) = \alpha \sinh^{\frac{2}{3}} \frac{3}{2} \tau, \quad (10)$$

where α is a free parameter that we can set to whatever value we wish, since the degree distribution does not depend on it, see Section III E. We wish to set α to the value such that the generated causet would have a desired number of nodes

$$N = \frac{1}{3} \pi^2 \delta \alpha^3 (\sinh 3\tau_0 - 3\tau_0), \quad (11)$$

where δ , the node density, is yet another free parameter that does not affect the degree distribution according to Section III E. The scale factor in Eq. (10) means that the temporal coordinate that we assign to each of these N nodes is a random number $\tau \in [0, \tau_0]$ drawn from distribution

$$\rho(\tau|\tau_0) = \frac{6 \sinh^2 \frac{3}{2} \tau}{\sinh 3\tau_0 - 3\tau_0}. \quad (12)$$

Having times τ assigned, we then map them, for each node, to conformal times η via

$$\eta = \frac{2}{3\alpha} \int_0^{\frac{3}{2}\tau} \frac{dx}{\sinh^{\frac{2}{3}} x}. \quad (13)$$

The spatial coordinates θ , θ_1 , and θ_2 are then assigned exactly as in the previous section, and the causet network is also formed exactly the same way, i.e. by future→past linking all node pairs whose temporal distance $\Delta\eta$ exceeds their spatial distance $\Delta\theta$.

Figure 4 shows the in-degree distribution for a causet generated with $\alpha = 2.01$ and $\delta = 10^4$. The resulting number of nodes in the causet is $N = 10^6$. The analytic solution curves are obtained using the approximations for the in-degree distribution derived in Section III. The key equations are Eq. (70), yielding the Laplace approximation for the

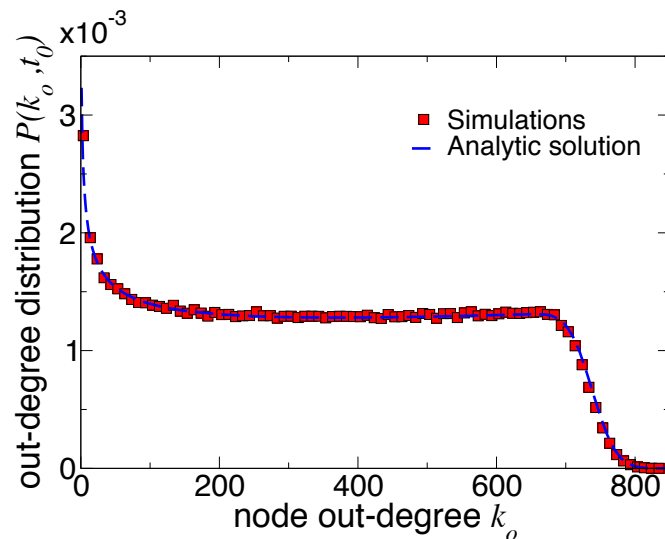


FIG. 6: Out-degree distribution in the simulated universe.

in-degree distribution, and Eq. (91) expressing conformal time as a function of the current value of the scale factor. The precise steps to numerically compute the analytic solution for the in-degree distribution are listed in Section III G. The perfect match between the simulations and analytic solution in Fig. 4 confirms that the approximations used in Section III to derive the analytic solution yield very accurate results.

The out-degree distribution in the same simulated causet is shown in Fig. 6. The analytic solution is obtained by numeric evaluations of Eqs.(62-66). The distribution appears to be uniform over a wide range of degree values.

II. ASYMPTOTIC EQUIVALENCE BETWEEN CAUSAL SETS IN DE SITTER SPACETIME AND COMPLEX NETWORKS IN HYPERBOLIC SPACE

A. De Sitter spacetime

The $d + 1$ -dimensional de Sitter spacetime [16] is the exact solution of the Einstein equations

$$G_{\mu\nu} + \Lambda g_{\mu\nu} = 0 \quad (14)$$

for the empty universe with positive vacuum energy density. In these equations, $G_{\mu\nu} = R_{\mu\nu} - \frac{1}{2}Rg_{\mu\nu}$ is the Einstein tensor, $R_{\mu\nu}$ the Ricci tensor, R the scalar curvature, $g_{\mu\nu}$ the metric tensor, Λ the cosmological constant, and all the notations are in the natural units with the speed of light $c = 1$. This spacetime can be represented as the one-sheeted $d + 1$ -dimensional hyperboloid of constant positive scalar R and Gaussian K curvatures [32]

$$-z_0^2 + z_1^2 + \dots + z_{d+1}^2 = a^2 = \frac{d(d-1)}{2\Lambda} = \frac{d(d+1)}{R} = \frac{1}{K} \quad (15)$$

borrowing its metric from the $d + 2$ -dimensional ambient Minkowski space with metric

$$ds^2 = -dz_0^2 + dz_1^2 + \dots + dz_{d+1}^2. \quad (16)$$

This hyperboloid in the $d = 1$ case is visualized as the outer hyperboloid in Fig. 2. As a side note, the curvature of the same hyperboloid in the Euclidean metric is everywhere negative but not constant. For $d = 3$, the Hubble constant H , vacuum energy density ρ_Λ , cosmological constant Λ , and the hyperboloid pseudoradius a , scalar curvature R , and Gaussian curvature K are all related by

$$H^2 = \frac{8}{3}\pi G\rho_\Lambda = \frac{\Lambda}{3} = \frac{1}{a^2} = \frac{R}{12} = K, \quad (17)$$

where G is the gravitational constant.

De Sitter spacetime admits different natural coordinate systems with negative, zero, or positive *spatial* curvatures, which are not to be confused with the positive curvature of the whole *spacetime*. Here we use the standard coordinate system $(t, \theta_1, \dots, \theta_d)$ with positive spatial curvature that covers the whole spacetime:

$$z_0 = a \sinh \frac{t}{a}, \quad (18)$$

$$z_1 = a \cosh \frac{t}{a} \cos \theta_1, \quad (19)$$

⋮

$$z_d = a \cosh \frac{t}{a} \sin \theta_1 \dots \sin \theta_{d-1} \cos \theta_d, \quad (20)$$

$$z_{d+1} = a \cosh \frac{t}{a} \sin \theta_1 \dots \sin \theta_{d-1} \sin \theta_d, \quad (21)$$

where $t \in \mathbb{R}$ is the cosmological time of the universe, and $\theta_1, \dots, \theta_{d-1} \in [0, \pi]$ and $\theta_d \in [0, 2\pi]$ are the standard angular coordinates on the unit d -dimensional sphere \mathbb{S}^d . The time t at spacetime point P is also the Minkowski length of the arc connecting P to the corresponding point at time $t = 0$ belonging to the $z_0 = 0$ slice of the hyperboloid, see Fig. 2. In these coordinates the metric takes the Friedmann-Lemaître-Robertson-Walker (FLRW) form for an exponentially expanding homogeneous and isotropic universe with positive spatial curvature:

$$ds^2 = -dt^2 + a^2 \cosh^2 \frac{t}{a} (d\theta^2 + \sin^2 \theta d\Omega_{d-1}^2) = -dt^2 + a^2 \cosh^2 \frac{t}{a} d\Omega_d^2, \quad \text{where} \quad (22)$$

$$d\Omega_d^2 = d\theta_1^2 + \sin^2 \theta_1 d\theta_2^2 + \dots + \sin^2 \theta_1 \dots \sin^2 \theta_{d-1} d\theta_d^2 \quad (23)$$

is the metric on \mathbb{S}^d . That is, at each time t , the universe is a sphere of exponentially growing radius $a \cosh(t/a)$ and volume

$$v = \sigma_d \left(a \cosh \frac{t}{a} \right)^d, \quad \text{where } \sigma_d = \frac{2\pi^{\frac{d+1}{2}}}{\Gamma\left(\frac{d+1}{2}\right)} \quad (24)$$

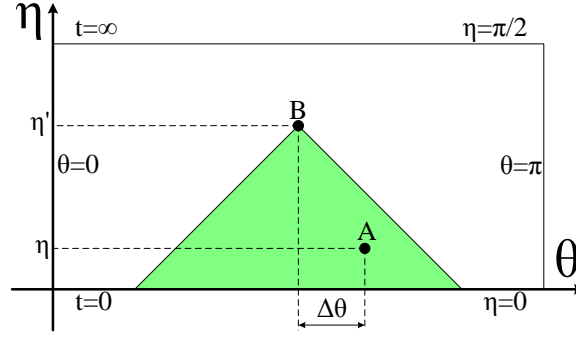


FIG. 7: Causal structure of the $d + 1$ -dimensional de Sitter spacetime. $d - 1$ dimensions are suppressed, so that each point represents a $d - 1$ -sphere. $\Delta\theta$ is the distance between A and B on the d -dimensional unit sphere \mathbb{S}^d .

is the volume of \mathbb{S}^d . Figure 2 visualizes this foliation for $d = 1$, in which case these time-slice spheres are circles, and their volume is the circle's circumference.

To study the causal structure of de Sitter spacetime, it is convenient to introduce conformal time $\eta \in (-\frac{\pi}{2}, \frac{\pi}{2})$ via

$$\cos \eta = \frac{1}{\cosh \frac{t}{a}}. \quad (25)$$

These conformal-time coordinates are convenient because the metric becomes

$$ds^2 = \frac{a^2}{\cos^2 \eta} (-d\eta^2 + d\theta^2 + \sin^2 \theta d\Omega_{d-1}^2), \quad (26)$$

so that the light cone boundaries defined by $\Delta s = 0$ are straight lines at 45° with the (η, θ) axes, see Fig. 7. Therefore, in this figure, point A at time $\eta \in [0, \eta']$ lies in the past light cone of point B at time $\eta' \in (0, \pi/2)$ if the angular distance $\Delta\theta$ between A and B on \mathbb{S}^d is less than the conformal time difference $\eta' - \eta$ between them:

$$\Delta\theta < \eta' - \eta = \arccos \frac{1}{\cosh \frac{t'}{a}} - \arccos \frac{1}{\cosh \frac{t}{a}}, \quad \text{or approximately} \quad (27)$$

$$\Delta\theta < 2 \left(e^{-\frac{t}{a}} - e^{-\frac{t'}{a}} \right) \approx 2e^{-\frac{t}{a}}, \quad (28)$$

where the last approximation holds for $t' \gg t \gg 1$, and where we have used the approximation $\eta = \arccos[1/\cosh(t/a)] \approx \pi/2 - 2e^{-t/a}$, which is valid for large t .

The volume form on de Sitter spacetime in the conformal and cosmological time coordinates is given by

$$dV = \left(\frac{a}{\cos \eta} \right)^{d+1} d\eta d\Phi_d = \left(a \cosh \frac{t}{a} \right)^d dt d\Phi_d \approx \left(\frac{a}{2} \right)^d e^{\frac{d}{a}t} dt d\Phi_d, \quad \text{where} \quad (29)$$

$$d\Phi_d = \sin^{d-1} \theta_1 \sin^{d-2} \theta_2 \dots \sin \theta_{d-1} d\theta_1 d\theta_2 \dots d\theta_d \quad (30)$$

is the volume form on \mathbb{S}^d , i.e. $\int d\Phi_d = \sigma_d$.

B. Hyperbolic space

The hyperboloid model of the $d + 1$ -dimensional hyperbolic space [33] is represented by one sheet of the two-sheeted $d + 1$ -dimensional hyperboloid of constant negative scalar R and Gaussian K curvatures

$$-z_0^2 + z_1^2 + \dots + z_{d+1}^2 = -b^2 = \frac{d(d+1)}{R} = \frac{1}{K} \quad (31)$$

borrowing its metric from the $d + 2$ -dimensional ambient Minkowski space with metric (16). This hyperboloid in the $d = 1$ case is visualized as the inner hyperboloid in Fig. 2. As a side note, the curvature of the same hyperboloid in

the Euclidean metric is everywhere positive but not constant. The standard coordinate system $(r, \theta_1, \dots, \theta_d)$ on this hyperboloid is given by

$$z_0 = b \cosh \frac{r}{b}, \quad (32)$$

$$z_1 = b \sinh \frac{r}{b} \cos \theta_1, \quad (33)$$

$$\vdots$$

$$z_d = b \sinh \frac{r}{b} \sin \theta_1 \dots \sin \theta_{d-1} \cos \theta_d, \quad (34)$$

$$z_{d+1} = b \sinh \frac{r}{b} \sin \theta_1 \dots \sin \theta_{d-1} \sin \theta_d, \quad (35)$$

where $r \in \mathbb{R}_+$ is the radial coordinate, and $\theta_1, \dots, \theta_{d-1} \in [0, \pi]$ and $\theta_d \in [0, 2\pi]$ are the standard angular coordinates on the unit d -dimensional sphere \mathbb{S}^d . The radial coordinate r of point P on the hyperboloid is the Minkowski length of the arc connecting P to the hyperboloid vertex, which is the bottom of the inner hyperboloid in Fig. 2. As a side note, the Euclidean length r_E of the same arc is given by the incomplete elliptic integral of the second kind $r_E = -iE(ir, 2)$.

C. Hyperbolic model of complex networks

In the hyperbolic model of complex networks [18], networks grow over the $d + 1$ dimensional hyperbolic space of Gaussian curvature $K = -1/b^2$ according to the following rule in the simplest case. New nodes n are born one at a time, $n = 1, 2, 3, \dots$, so that n can be called a network time. Each new node is located at a random position on \mathbb{S}^d . That is, the angular coordinates $(\theta_1, \dots, \theta_d)$ for new nodes are drawn from the uniform distribution on \mathbb{S}^d . The radial coordinate of the new node is

$$r = 2 \frac{b}{d} \ln \frac{n}{\nu}, \quad (36)$$

where ν is a parameter controlling the average degree in the network. Upon its birth, each new node connects to all the nodes lying within hyperbolic distance r from itself. In other words, the connectivity perimeter of new node n at time n is the hyperbolic ball of radius r centered at node n . The hyperbolic distance x between two points with radial coordinates r and r' located at angular distance $\Delta\theta$ is given by the hyperbolic law of cosines [33]:

$$x = b \operatorname{arccosh} \left(\cosh \frac{r}{b} \cosh \frac{r'}{b} - \sinh \frac{r}{b} \sinh \frac{r'}{b} \cos \Delta\theta \right) \approx r + r' + 2b \ln \frac{\Delta\theta}{2}. \quad (37)$$

Therefore new node n' connects to existing nodes $n < n'$ whose coordinates satisfy

$$\begin{aligned} x &< r', \quad \text{or approximately} & (38) \\ r + 2b \ln \frac{\Delta\theta}{2} &< 0. & (39) \end{aligned}$$

This construction yields growing networks whose distribution $P(k)$ of node degrees k is a power law, $P(k) \sim k^{-\gamma}$, with $\gamma = 2$. Indeed, according to Eq. (36), the radial density of nodes at any given time scales with r as $\rho(r) \sim e^{\alpha r}$, where $\alpha = d/(2b)$. One can also calculate, see [34], the average degree of nodes at radial coordinate r , which is $\bar{k}(r) \sim e^{-\beta r}$, where $\beta = \alpha$. The probability that a node at r has degree k is given by the Poisson distribution with the mean equal to $\bar{k}(r)$. Taken altogether, these observations prove that $\gamma = \alpha/\beta + 1 = 2$. The networks in the model also have strongest possible clustering, i.e. the largest possible number of triangular subgraphs, for graphs with this degree distribution, and their average degree is

$$\bar{k} \approx 2^{d+1} \frac{v_d}{\sigma_d} \nu \ln n, \quad \text{where } v_d = \frac{\sigma_{d-1}}{d} \quad (40)$$

is the volume of the unit d -dimensional ball. The model and its extensions describe the large-scale structure and growth dynamics of different real networks, e.g. the Internet, metabolic networks, and social networks, with a remarkable accuracy [18].

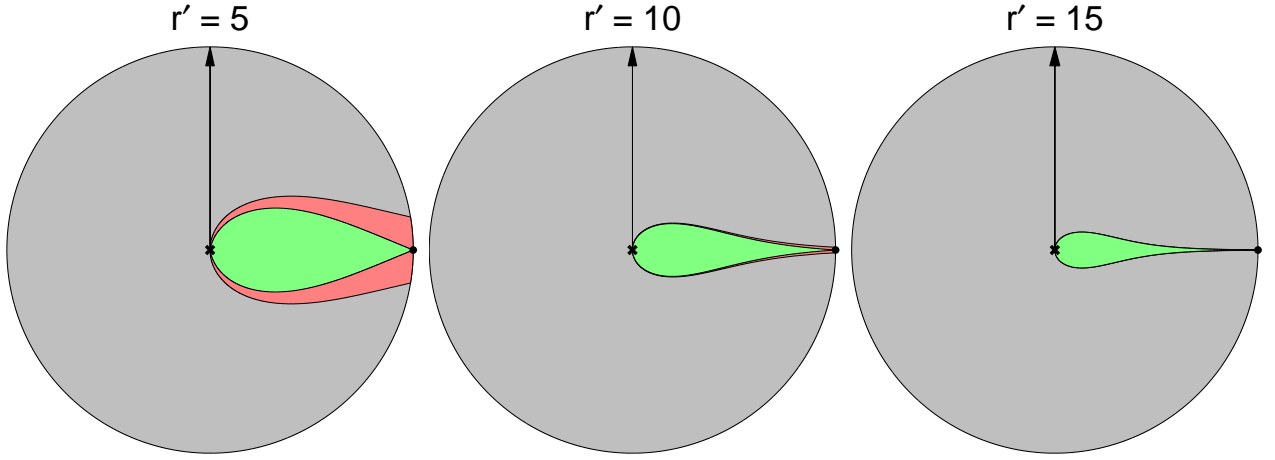


FIG. 8: The hyperbolic disc (red) given by Eq. (38) of time radius $r' = t'$ centered at the black point representing a new node in Section II C vs. its past de Sitter light cone (green) given by Eq. (27) for different values of r' in the $d = 1, b = 1$ case. Assuming the average degree of $\bar{k} = 10$, the shown time radii correspond to network sizes of approximately 40, 200, and 2000 nodes.

D. Duality between de Sitter causal sets and complex networks

To demonstrate the asymptotic equivalence between growing networks from the previous section and causal sets growing de Sitter spacetime, we:

1. find a mapping of points in the hyperbolic space \mathbb{H}^{d+1} to de Sitter spacetime $d\mathbb{S}^{d+1}$ such that:
2. the hyperbolic ball of new node $n \in \mathbb{H}^{d+1}$ is asymptotically identical to its past light cone in $d\mathbb{S}^{d+1}$ upon the mapping, and
3. the distribution of nodes after mapping is uniform in $d\mathbb{S}^{d+1}$.

1. Mapping

A mapping that, as we prove below, satisfies the properties above is remarkably simple:

$$t = r, \quad (41)$$

$$a = 2b. \quad (42)$$

That is, we identify radial coordinate r in \mathbb{H}^{d+1} with time t in $d\mathbb{S}^{d+1}$, keeping all the angular coordinates the same—see Fig. 2 for illustration.

2. Hyperbolic balls versus past light cones

The proof that the hyperbolic balls of new node connections map asymptotically to past light cones is trivial: inequalities (39) and (28) are identical with the mapping above. See Fig. 8 visualizing the approximation accuracy at different times.

3. Uniform node density

The proof that the node density after mapping is uniform in $d\mathbb{S}^{d+1}$ is trivial as well. Indeed, according to Eq. (36) with $2b = a$, network time n is related to cosmological time t via

$$n = \nu e^{\frac{a}{2}t}, \quad \text{so that} \quad (43)$$

$$dn = \nu \frac{d}{a} e^{\frac{a}{2}t} dt. \quad (44)$$

Using the last equation, we rewrite the de Sitter volume element in Eq. (29) as

$$dV = \frac{2b^{d+1}}{\nu d} dn d\Phi_d. \quad (45)$$

By construction in Section II C, the node density on \mathbb{S}^d is uniform and equal to 1. Therefore the number of nodes dN in element $dn d\Phi_d$ is

$$dN = \frac{1}{\sigma_d} dn d\Phi_d. \quad (46)$$

Combining the last two equations, we obtain

$$dN = \delta dV, \quad \text{where} \quad (47)$$

$$\delta = \frac{\nu d}{2b^{d+1}\sigma_d}, \quad (48)$$

meaning that nodes are distributed uniformly in $d\mathbb{S}^{d+1}$ with constant density δ , thus completing the proof.

A causal set growing in de Sitter spacetime with node density δ in Eq. (48) is thus asymptotically equivalent to a growing complex network in Section II C with average degree \bar{k} in Eq. (40). Combining these two equations, we can relate δ and \bar{k} to each other:

$$\bar{k} \approx 2\nu_d \delta a^d t. \quad (49)$$

An important consequence of this asymptotic equivalence is that the degree distribution in both cases is the same power law with exponent $\gamma = 2$.

III. THE UNIVERSE AS A CAUSAL SET

De Sitter spacetime is the spacetime of a universe with positive vacuum (dark) energy density and no matter or radiation. Since the real universe does contain matter, its spacetime deviates from the pure de Sitter spacetime. At early times, matter dominates, leading to the Big Bang singularity at $t = 0$ that de Sitter spacetime lacks. At later times, the matter density decreases, while the dark energy density stays constant, so that it starts dominating, and the universe becomes asymptotically de Sitter. The universe today is at the crossover between the matter-dominated and dark-energy-dominated eras, since the matter and dark energy densities ρ_M and ρ_Λ are of the same order of magnitude, leading to rescaled cosmological time $\tau = t/a \sim 1$ —the so-called “*why now?*” puzzle in cosmology [24–26].

To quantify these deviations from pure de Sitter spacetime, and their effect on the structure of the causal set of the real universe, we calculate its degree distribution in this section. This task is quite challenging, and in what follows we first provide the exact analytic expression for the degree distribution, and then derive its approximations based on the measured properties of the universe. These approximations turn out to be remarkably accurate because according to the current measurements, the universe is almost flat.

We emphasize that the approximations in this section are based on the exact solution of the Einstein equations for a flat universe containing only matter and constant positive vacuum energy, i.e. constant cosmological constant Λ , and that we assume that the universe is governed by this solution at all times. This assumption is a simplification of reality for a number of reasons. For example, there are a plenty of cosmological scenarios, such as cosmic bubble collisions [35], in which the ultimate fate of the universe deviates from the asymptotic solution for the universe today. There are also a variety of models with non-constant Λ , yet the standard Λ CDM model with constant Λ is a base line describing accurately many observed properties of the real universe [36], partly justifying our simplifying assumption. We also note that by relying on the exact solution for a universe containing only matter and Λ , we effectively neglect the earliest stages of universe evolution such as the radiation-dominated era or inflationary epoch. There is no consensus on how exactly the universe evolved at those earliest times, but since the radiation-dominated era ended soon after the Big Bang [37], these details unlikely have a profound effect on the universe causet’s structure at much later times.

A. Exact expression for the degree distribution

The metric in a homogeneous and isotropic universe takes the FLRW form:

$$ds^2 = -dt^2 + R^2(t) \left\{ d\chi^2 + \frac{1}{K} \sin^2 \left[\sqrt{K} \chi \right] \left(\sin^2 \theta d\theta^2 + d\phi^2 \right) \right\}, \text{ where} \quad (50)$$

$$\frac{1}{K} \sin^2 \sqrt{K} \chi = \begin{cases} \sin^2 \chi & \text{if } K = 1 \text{ (closed universe with positive spatial curvature),} \\ \chi^2 & \text{if } K = 0 \text{ (flat universe with zero spatial curvature),} \\ \sinh^2 \chi & \text{if } K = -1 \text{ (open universe with negative spatial curvature).} \end{cases} \quad (51)$$

In the above expression, coordinates $\phi \in [0, 2\pi]$ and $\theta \in [0, \pi]$ are the standard angular coordinates on \mathbb{S}^2 , while $\chi \in [0, \pi]$ if $K = 1$, or $\chi \in [0, \infty]$ if $K = 0, -1$, is the radial coordinate in a spherical, flat, or hyperbolic space. Finally, $t \in [0, \infty]$ is the cosmological time, and $R(t)$ is the scale factor, finding an appropriate approximation to which in the real universe is an important part of our approximations in subsequent sections. In this and the next sections, however, all the expressions are valid for *any* scale factor.

As with pure de Sitter, it is convenient to introduce conformal time η , related to cosmological time t via

$$\eta = \int_0^t \frac{dt'}{R(t')}. \quad (52)$$

In conformal time coordinates, the metric and volume form become

$$ds^2 = R^2(\eta) \left\{ -d\eta^2 + d\chi^2 + \frac{1}{K} \sin^2 \left[\sqrt{K} \chi \right] \left(\sin^2 \theta d\theta^2 + d\phi^2 \right) \right\}, \quad (53)$$

$$dV = \frac{1}{K} R^4(\eta) \sin^2 \left[\sqrt{K} \chi \right] \sin \theta d\eta d\chi d\theta d\phi. \quad (54)$$

As with pure de Sitter, we orient edges in the universe’s causet from future to the past. Therefore if η is the current conformal time, then the average in- and out-degrees $\bar{k}_{i,o}(\eta'|\eta)$ of nodes born at conformal time $\eta' < \eta$ are simply

proportional to the volumes of their future and past light cones $V_{f,p}(\eta'|\eta)$:

$$\bar{k}_i(\eta'|\eta) = \delta V_f(\eta'|\eta), \quad (55)$$

$$\bar{k}_o(\eta'|\eta) = \delta V_p(\eta'|\eta), \quad (56)$$

where the coefficient of proportionality is the Planck-scale node density in the spacetime, which we take to be the inverse of the Planck 4-volume:

$$\delta = \frac{1}{t_P^4} = 1.184 \times 10^{173} \text{ s}^{-4}, \text{ where} \quad (57)$$

$$t_P = 5.391 \times 10^{-44} \text{ s} \quad (58)$$

is the Planck time.

Thanks to conformal time coordinates, the expressions for volumes $V_{f,p}(\eta'|\eta)$ are easy to write down:

$$V_f(\eta'|\eta) = \frac{1}{K} \int_{\eta'}^{\eta} d\eta'' R^4(\eta'') \int_0^{\eta''-\eta'} d\chi \sin^2[\sqrt{K}\chi] \int_0^{\pi} d\theta \sin\theta \int_0^{2\pi} d\phi, \quad (59)$$

$$V_p(\eta'|\eta) = \frac{1}{K} \int_0^{\eta'} d\eta'' R^4(\eta'') \int_0^{\eta'-\eta''} d\chi \sin^2[\sqrt{K}\chi] \int_0^{\pi} d\theta \sin\theta \int_0^{2\pi} d\phi. \quad (60)$$

Computing the three inner integrals, we obtain

$$\bar{k}_i(\eta'|\eta) = \delta \frac{\pi}{K} \int_{\eta'}^{\eta} \left\{ 2(\eta'' - \eta') - \frac{1}{\sqrt{K}} \sin[2\sqrt{K}(\eta'' - \eta')] \right\} R^4(\eta'') d\eta'', \quad (61)$$

$$\bar{k}_o(\eta'|\eta) = \delta \frac{\pi}{K} \int_0^{\eta'} \left\{ 2(\eta' - \eta'') - \frac{1}{\sqrt{K}} \sin[2\sqrt{K}(\eta' - \eta'')] \right\} R^4(\eta'') d\eta''. \quad (62)$$

As shown in [11], Lorentz invariance implies that nodes/events of the causet are distributed in spacetime according to a Poisson point process. Therefore, as explained in [38], to find the in- or out-degree distributions $P(k, \eta)$ at time η , we have to average the Poisson distribution

$$p(k|\eta', \eta) = \frac{1}{k!} [\bar{k}(\eta'|\eta)]^k e^{-\bar{k}(\eta'|\eta)}, \quad (63)$$

which is the probability that a node born at time η' has degree k , with the density of nodes born at time η'

$$\rho(\eta'|\eta) = \frac{R^4(\eta')}{\mathcal{N}(\eta)}, \text{ where} \quad (64)$$

$$\mathcal{N}(\eta) = \int_0^{\eta} R^4(\eta') d\eta' \quad (65)$$

is the time-dependent normalization factor. The result is

$$P(k, \eta) = \int_0^{\eta} p(k|\eta', \eta) \rho(\eta'|\eta) d\eta' = \frac{1}{\mathcal{N}(\eta)} \frac{1}{k!} \int_0^{\eta} [\bar{k}(\eta'|\eta)]^k e^{-\bar{k}(\eta'|\eta)} R^4(\eta') d\eta'. \quad (66)$$

The above expressions are valid for both in-degree (set $k \equiv k_i$ and $\bar{k}(\eta'|\eta) \equiv \bar{k}_i(\eta'|\eta)$) and out-degree ($k \equiv k_o$, $\bar{k}(\eta'|\eta) \equiv \bar{k}_o(\eta'|\eta)$) distributions. In what follows we focus on the in-degree distribution.

B. First approximation using the Laplace method

Equations (66,61) give the exact solution for the in-degree distribution with an arbitrary scale factor $R(\eta)$, but it is difficult to extract any useful information from these expressions, even if we know the exact form of $R(\eta)$. The first step to get a better insight into the causet properties is to rewrite $\bar{k}_i(\eta'|\eta)$ as

$$\bar{k}_i(\eta'|\eta) = \bar{k}_i(0|\eta) F(\eta'|\eta), \quad \text{where } F(\eta'|\eta) = \frac{\bar{k}_i(\eta'|\eta)}{\bar{k}_i(0|\eta)}. \quad (67)$$

The in-degree of the oldest node $\bar{k}_i(0|\eta)$ is an astronomically large number, both because the node is old, so that its future light cone comprises a macroscopic portion of the 4-volume of the whole universe, and because the degree is proportional to huge δ . However, function $F(\eta'|\eta)$ is a monotonically decreasing function whose values lie in the interval $[0, 1]$. We can thus use the Laplace method to approximate the integral in Eq. (66) in the limit $\delta \gg 1$. Introducing $\eta^*(k_i)$, which is the solution of the transcendent equation

$$k_i = \bar{k}_i(\eta^*|\eta), \quad (68)$$

and function

$$\Phi(k_i, \eta) = \left| \frac{\partial \bar{k}_i(\eta'|\eta)}{\partial \eta'} \right|_{\eta'=\eta^*(k_i)}, \quad (69)$$

the result of this Laplace approximation reads:

$$P(k_i, \eta) = \begin{cases} \left(\frac{3}{\pi\delta}\right)^{\frac{1}{4}} \Gamma\left(\frac{5}{4}\right) \frac{R^3(\eta)}{\mathcal{N}(\eta)} & \text{if } k_i = 0, \\ \frac{1}{\mathcal{N}(\eta)} \frac{\sqrt{2\pi\bar{k}_i} k_i^{k_i} e^{-k_i}}{k_i!} \frac{R^4[\eta^*(k_i)]}{\Phi(k_i, \eta)} \approx \frac{1}{\mathcal{N}(\eta)} \frac{R^4[\eta^*(k_i)]}{\Phi(k_i, \eta)} & \text{if } 1 \leq k_i \leq \bar{k}_i(0|\eta), \end{cases} \quad (70)$$

where we have also used Stirling's approximation $k! \approx \sqrt{2\pi k}(k/e)^k$. We see that the shape of the degree distribution is almost fully determined by $\eta^*(k_i)$, and that the distribution is a fast decaying function for degrees above $\bar{k}_i(0|\eta)$.

The expression for the in-degree distribution in Eq. (70) is now more tractable and gets ready to accept the scale factor $R(\eta)$ of the universe. Unfortunately, the exact expressions for the scale factor of a closed or open universe with matter and dark energy, although known [39], resist analytic treatment, and so does the integral for the average degree $\bar{k}_i(\eta'|\eta)$ in Eq. (61) that we are to use in Eq. (70). Therefore we next develop a series of approximations to the scale factor and average degree, based on the measured properties of the universe.

C. Measured properties of the universe

The current measurements of the universe [36] that are relevant to us here include:

$$\Omega_\Lambda = \frac{8\pi G}{3H_0^2} \rho_\Lambda \in [0.709, 0.741], \quad (\text{dark energy density}) \quad (71)$$

$$\Omega_M = \frac{8\pi G}{3H_0^2} \rho_M \in [0.2582, 0.2914], \quad (\text{matter density}) \quad (72)$$

$$\Omega_K = -\frac{K}{R_0^2 H_0^2} \in [-0.0133, 0.0084], \quad (\text{curvature density}), \quad \text{where} \quad (73)$$

$$H_0 = \frac{\dot{R}_0}{R_0} \in [68.8, 71.6] \frac{\text{km}}{\text{s} \cdot \text{Mpc}} = [2.23, 2.32] \times 10^{-18} \text{ s}^{-1} \text{ is the Hubble constant,} \quad (74)$$

$$R_0 = R(t_0) \text{ is the scale factor at present time } t_0, \text{ i.e. the age of the universe,} \quad (75)$$

$$t_0 \in [13.65, 13.87] \text{ Gyr} = [4.308, 4.377] \times 10^{17} \text{ s, so that} \quad (76)$$

$$\Lambda = 3H_0^2 \Omega_\Lambda \in [1.06, 1.20] \times 10^{-35} \text{ s}^{-2}, \text{ is the cosmological constant, and} \quad (77)$$

$$a = \sqrt{\frac{3}{\Lambda}} = \frac{1}{\sqrt{\Omega_\Lambda} H_0} \in [5.00, 5.32] \times 10^{17} \text{ s, is the de Sitter pseudoradius.} \quad (78)$$

The range of values of Ω_Λ , Ω_M , H_0 , and t_0 are given by the 95% confidence bounds in the universe measurements taken from the last column of Table 1 in [36], while the values of Ω_K come from Table 2 there: third row, last column. The matter density Ω_M is the sum of two contributions: the observable (baryon) matter density ($\Omega_b \in [0.0442, 0.0474]$), and dark matter density ($\Omega_c \in [0.214, 0.244]$). The radiation density is negligible. The universe thus consists of dark energy ($\approx 73\%$), dark matter ($\approx 23\%$), and observable matter ($\approx 4\%$). As a side note, the sum of all Ω 's $\sum \Omega \in [0.95, 1.04]$ as expected, since $\sum \Omega = 1$ is the Einstein/Friedmann equation for a FLRW universe, which we recall in the next section. Much more important for us here is that the universe is almost flat, $\Omega_K \approx 0$.

D. Approximations to the scale factor and average degree

In this section we utilize the approximate flatness of the universe to derive and quantify approximations to the scale factor of the universe and average degree in Eq. (61). The main idea is that since Ω_K is small, we can use the exact solution for the scale factor in a flat universe ($\Omega_K = 0$) with matter and dark energy (positive cosmological constant), which is actually quite simple [16].

We first recall that the 00-component of the Einstein equations in the FLRW metric is the first Friedmann equation:

$$\frac{\dot{R}^2 + K}{R^2} = \frac{8}{3}\pi G \left[\rho_\Lambda + \left(\frac{R_0}{R}\right)^3 \rho_M \right]. \quad (79)$$

This equation can be rewritten [40] in the following form:

$$H_0 t = \int_0^{R/R_0} \frac{dx}{x\sqrt{\Omega_\Lambda + \Omega_K x^{-2} + \Omega_M x^{-3}}}. \quad (80)$$

Assuming non-vanishing positive dark energy and matter densities ($\Omega_\Lambda > 0$ and $\Omega_M > 0$), using rescaled time

$$\tau \equiv \frac{t}{a}, \quad (81)$$

and introducing two parameters

$$\alpha \equiv R_0 \sqrt[3]{\frac{\Omega_M}{\Omega_\Lambda}}, \text{ and} \quad (82)$$

$$\epsilon \equiv \frac{\Omega_K}{\sqrt[3]{\Omega_\Lambda \Omega_M^2}} \in [-0.0368, 0.0232], \quad (83)$$

the integral in Eq. (80) simplifies to

$$\tau = \int_0^r \frac{dx}{x\sqrt{1 + \epsilon x^{-2} + x^{-3}}}. \quad (84)$$

Solving it for $r \equiv r(\tau, \epsilon)$, we conclude that the solution for the scale factor becomes

$$R(t) = \alpha r(\tau; \epsilon). \quad (85)$$

This is definitely not the only way to write down the scale factor in terms of the parameters of the universe. Yet written in this form, the rescaled scale factor $r(\tau; \epsilon)$ is a dimensionless function of its dimensionless arguments, and parameter ϵ is close to zero, so that $r(\tau; \epsilon) \approx r(\tau; 0)$, where $r(\tau, 0)$, i.e. the rescaled scale factor for a flat universe with positive matter and dark energy densities, is quite simple:

$$r(\tau; 0) = \sinh^{\frac{2}{3}} \frac{3}{2} \tau. \quad (86)$$

Figure 9(left) shows a good agreement between the numerical solution for $r(\tau; \epsilon)$ and the analytical expression for $r(\tau; 0)$ in Eq. (86) for the range of the values of ϵ allowed by measurements in Eq (83). Therefore in what follows we can use Eq. (86), even if the universe is “slightly closed” or “slightly open.”

To approximate the average degree $\bar{k}_i(\eta'|\eta)$ in Eq. (61), we first compute, using the scaling Eq. (85), the conformal time

$$\eta = \int_0^t \frac{dt'}{R(t')} = \sqrt{|\epsilon|} \int_0^\tau \frac{d\tau'}{r(\tau'; \epsilon)} = \sqrt{|\epsilon|} \int_0^{r(\tau; \epsilon)} \frac{dx}{x^2 \sqrt{1 + \epsilon x^{-2} + x^{-3}}} \quad (87)$$

at the future infinity $t = \tau = r(\tau; \epsilon) = \infty$. For the extreme values of ϵ allowed by measurements, we obtain $\eta_\infty = 0.5403$ for the closed universe with $\epsilon = -0.0368$ and $\eta_\infty = 0.4260$ for the open universe with $\epsilon = 0.0232$. If $\epsilon \rightarrow 0$, then we also have $\eta_\infty \rightarrow 0$, yet if ϵ is exactly zero, then η_∞ is an undefined constant, since in the flat case, R_0 is a free parameter that can be set to an arbitrary value without affecting anything. If the universe is not exactly flat,

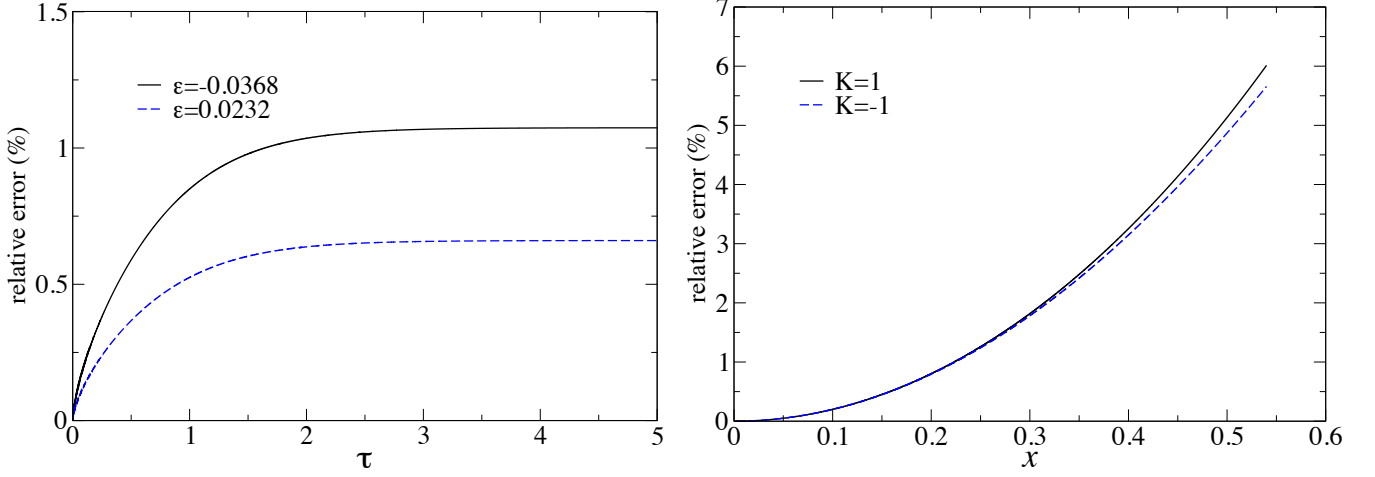


FIG. 9: Left: Relative error between functions $r(\tau; \epsilon)$ and $r(\tau; 0)$, $|r(\tau; \epsilon) - r(\tau; 0)|/r(\tau; \epsilon)$, for the two extremes of the 95% confidence interval of parameter ϵ in Eq. (83), as a function of rescaled time τ . In the worst case, the relative error is around 1%. Right: Relative error of approximation in Eq. (88) for $x \in [0, \eta_\infty]$.

then the above values of η_∞ allowed by measurements are well below $\pi/2$, so that we can safely replace expression $[2x - \sin(2\sqrt{K}x)/\sqrt{K}]/K$ in Eq. (61) by its Taylor expansion around zero,

$$\frac{1}{K} \left[2x - \frac{1}{\sqrt{K}} \sin(2\sqrt{K}x) \right] \approx \frac{4}{3} x^3. \quad (88)$$

Indeed the maximum possible relative error between the left and right hand sides in the last equation at $x = \eta_\infty$ is around 6%, see Fig. 9(right), whereas such error is zero for an exactly flat universe with $\epsilon = K = 0$, since the left and right hand sides are equal in this case. Therefore the approximation to the average degree in Eq. (61)

$$\bar{k}_i(\eta'|\eta) = \frac{4}{3} \pi \delta \int_{\eta'}^{\eta} (\eta'' - \eta')^3 R^4(\eta'') d\eta'' \quad (89)$$

is exact for flat universes, and almost exact for slightly closed or open universes with ϵ within the range of Eq. (83).

E. Scaling relations

To proceed to our final approximations to the degree distribution in the next section, we derive some scaling relations that tremendously simplify the calculations, provide important insights into the properties of the degree distribution, and suggest methods to simulate the causal set of the universe.

We begin with the scaling relation for conformal time η . Let us introduce the rescaled conformal time

$$\zeta \equiv \frac{\alpha}{a} \eta = \frac{\eta}{\sqrt{|\epsilon|}}, \quad (90)$$

and let notations $y = f_{1,2,\dots}(x)$ mean “ y is a function of x .” Given the definition of conformal time in Eq. (87), this rescaled conformal time is a function of rescaled cosmological time τ :

$$\zeta = f_1(\tau) = \int_0^{r(\tau; \epsilon)} \frac{dx}{x^2 \sqrt{1 + \epsilon x^{-2} + x^{-3}}} \xrightarrow{\epsilon \rightarrow 0} 2\sqrt{r(\tau; 0)} {}_2F_1\left(\frac{1}{6}, \frac{1}{2}, \frac{7}{6}, -r^3(\tau; 0)\right), \quad (91)$$

where $r(\tau; 0)$ is given by Eq. (86), and ${}_2F_1$ is the hypergeometric function. This scaling means that

$$R(\eta) = \alpha f_2(\zeta), \quad (92)$$

which in turn implies that the average in-degree of nodes born at time η'

$$\bar{k}_i(\eta'|\eta) = q f_3(\zeta', \zeta) = q f_4(\tau', \tau), \quad \text{where} \quad (93)$$

$$q \equiv \delta a^4, \quad (94)$$

while the average in- or out-degree in the causet

$$\bar{k}_i(\eta) = \bar{k}_o(\eta) = \int_0^{\eta_\infty} \bar{k}_i(\eta'|\eta) \rho(\eta'|\eta) d\eta' = qf_5(\zeta) = qf_6(\tau). \quad (95)$$

Plugging scaling Eqs. (93,94) into the expression for the in-degree distribution in Eq. (70), we conclude that this distribution scales for $k_i \geq 1$ as

$$P(k_i, t) = \frac{1}{q} Q(\kappa_i, \tau), \quad \text{where} \quad (96)$$

$$\kappa_i \equiv \frac{k_i}{q}, \quad (97)$$

and the rescaled in-degree distribution $Q(\kappa_i, \tau)$ is some function of rescaled degree κ_i and time τ . This result is important for several reasons:

1. It defines a characteristic degree $q = \delta a^4$ and characteristic time a such that the degree distribution depends only on the rescaled dimensionless variables $\kappa_i = k_i/q$ and $\tau = t/a$. Therefore we are free to set $a = 1$ and $\delta = 1$, and the remaining task is to find an explicit form of the rescaled distribution $Q(\kappa_i, \tau)$ in Eq. (96).
2. Even though the scale factor in Eq. (85) does depend on α , the in-degree distribution $P(k_i, t)$ does not depend on α . This is important from the practical point of view, because we can carry out all the calculations setting $\alpha = 1$ as well.
3. Having set $\alpha = a = \delta = 1$, the in-degree distribution explicitly does not depend on any physical parameters of the universe. The causets in flat or open universes are graphs with obviously infinite numbers of nodes from the very beginning of the universe, while the causets of closed universes are always finite, and the number of nodes in them depend on time and on all the three parameters α , a , and δ . Yet the in-degree distributions in all these causets at a given time are all the same, and in particular, do not depend on the number of nodes at all. This somewhat unexpected result deserves further explanation. We note that parameter $\alpha = R_0 \sqrt[3]{\Omega_M/\Omega_\Lambda}$ depends on the physical properties of the universe. In particular, if the universe is closed, it defines, via R_0 in Eq. (73), the radius of the three-sphere, i.e. of the spatial part of the FLRW metric. Since the degree distribution does not depend on α , we can freely take the limit $\alpha \rightarrow \infty$ corresponding to a flat space, without affecting the degree distribution. In other words, we are free to choose a closed universe with $K = +1$ in Eq. (50), and this choice can be considered as a degree-distribution-preserving compactification of an infinite flat or hyperbolic space with an infinite number of nodes in it, into a compact spherical space with a finite number of nodes.
4. The previous point informs us how to simulate the universe causet on a computer. We cannot simulate infinite causets for flat or open universes, but since the degree distribution is the same in closed universes, we are free to simulate the latter. One can check that in a closed universe, the number of nodes in a causet grows with time as

$$N(t) = \delta a \alpha^3 f_7(\tau). \quad (98)$$

We can set $a = 1$, and since the in-degree distribution does not depend on the number of nodes N , then for any given time $t = a\tau = \tau$ and for any given value of δ , we can generate graphs with any desired size N by choosing the value of α accordingly. The degree distribution obtained from this simulation is then to be re-scaled according to Eq. (96) to obtain the rescaled distribution $Q(\kappa_i, \tau)$. Keeping fixed $t = \tau$ and N , we can also explore different regions of $Q(\kappa_i, \tau)$ by changing the value of δ .

We have to emphasize that the points above, and the scaling relations in this section, are valid for non-flat universes only when η_∞ is well below $\pi/2$, so that the approximation in Eq. (88) is valid for all $x \in [0, \eta_\infty]$. When this condition does not hold, e.g. when ϵ is large and the universe is far from being flat, then all these scaling relations break down. In particular, we cannot claim that in that case the in-degree distribution would still be the same. The latest measurements of the universe parameters indicate that the scaling laws derived in this section do apply to the real universe, but even if this were not the case, these laws would still be valid for small values of conformal time.

F. Final approximations to the degree distribution in the matter- and dark-energy-dominated eras

We now have all the material needed to derive the final approximations to the degree distribution. According to Section III D the exact solution for the scale factor in a flat universe is a good approximation for the scale factor in

the real universe within the measurement-allowed range of parameter values, so that we will use this approximation here, i.e. we set $\epsilon = 0$. Using the scaling results from Section III E, we also set $a = \alpha = \delta = 1$, which is equivalent to working with rescaled cosmological time τ , rescaled conformal time ζ , rescaled scale factor $r(\tau) = \sinh^{2/3}(3\tau/2)$, and rescaled in-degree κ_i . Since everything is rescaled in this section, we omit word “rescaled” in front of the variable names.

We consider two eras of the universe evolution. The first era characterizes the causal set of the universe at early times, when matter dominates. The second era deals with the aged universe at large times, when dark energy dominates. In the limit of infinite time (future infinity), we derive the exact solution for the degree distribution in a flat universe.

1. Matter-dominated era

In this era with $\tau \ll 1$, the scale factor and conformal time can be approximated by

$$r(\tau) = \left(\frac{3}{2}\tau\right)^{\frac{2}{3}} \quad (99)$$

$$\zeta = 2\left(\frac{3}{2}\tau\right)^{\frac{1}{3}}, \text{ so that} \quad (100)$$

$$r(\zeta) = \left(\frac{\zeta}{2}\right)^2. \quad (101)$$

Using these expressions in the rescaled version of Eq. (89), we obtain the average in-degree at time ζ of nodes born at time ζ' :

$$\bar{\kappa}_i(\zeta'|\zeta) = \frac{\pi}{768}\zeta^{12} \left[\frac{1}{12} - \frac{3}{11}\frac{\zeta'}{\zeta} + \frac{3}{10}\left(\frac{\zeta'}{\zeta}\right)^2 - \frac{1}{9}\left(\frac{\zeta'}{\zeta}\right)^3 + \frac{1}{1980}\left(\frac{\zeta'}{\zeta}\right)^{12} \right]. \quad (102)$$

The maximum average in-degree, i.e. the average in-degree of the oldest nodes, is

$$\bar{\kappa}_i(0|\zeta) = \frac{\pi}{9216}\zeta^{12} = 9\pi\tau^4. \quad (103)$$

We note that if we reinsert constants a and δ , and cosmological time t using Eq. (93), the average in-degree of the oldest nodes becomes

$$\bar{k}_i(0|t) = 9\pi \left(\frac{t}{t_P}\right)^4, \quad (104)$$

where t_P is the Planck time, see Eq. (57). As expected, this in-degree does not depend on a and, consequently, on the cosmological constant Λ .

For degrees well below the maximum degree, $\kappa_i \ll 9\pi\tau^4$, the Taylor expansion of Eq. (102) around $\zeta' = \zeta$ yields

$$\bar{\kappa}_i(\zeta'|\zeta) \approx \frac{\pi}{3072}\zeta^{12} \left(\frac{\zeta'}{\zeta} - 1\right)^4. \quad (105)$$

Using this expression in the rescaled version of Eq. (70), we obtain

$$Q(\kappa_i, \tau) = \frac{3}{4} \left(\frac{3}{\pi}\right)^{\frac{1}{4}} \frac{\kappa_i^{-3/4}}{\tau} \quad \text{if } \kappa_i \ll 9\pi\tau^4, \quad (106)$$

and, after reinserting all the physical constants,

$$P(k_i, t) = \frac{3}{4} \left(\frac{3}{\pi}\right)^{\frac{1}{4}} \frac{t_P}{t} k_i^{-3/4} \quad \text{if } 1 \leq k_i \ll 9\pi \left(\frac{t}{t_P}\right)^4, \quad (107)$$

with a soft cut-off at $9\pi(t/t_P)^4$. We thus observe that the degree distribution does not depend on the cosmological constant Λ , and that it is a power law $P(k_i, \tau) \sim k_i^{-\gamma}$ with exponent $\gamma = 3/4$.

2. Dark-energy-dominated era

We now analyze the future fate of the universe at $\tau \gg 1$, which is slightly more intricate. To begin, we derive a couple of expressions that we use in simulations and that are valid for any τ . We first recall that, according to Eq. (91), conformal time is related to the current value of the scale factor r via

$$\zeta(r) = 2\sqrt{r} {}_2F_1\left(\frac{1}{6}, \frac{1}{2}, \frac{7}{6}, -r^3\right), \quad (108)$$

which is a monotonously increasing function of r . Therefore we can use scale factor value r as a measure of time instead of ζ . Using this observation in Eq. (89), we write the average in-degree at time r of nodes born at time r' as

$$\bar{\kappa}_i(r'|r) = \frac{4\pi}{3} \int_{r'}^r [\zeta(x) - \zeta(r')]^3 \frac{x^2 dx}{\sqrt{1+x^{-3}}}. \quad (109)$$

Similarly, function $\Phi(\kappa_i, r)$ in Eq. (69) becomes

$$\Phi(\kappa_i, r) = 4\pi \int_{r^*(\kappa_i)}^r [\zeta(x) - \zeta(r^*(\kappa_i))]^2 \frac{x^2 dx}{\sqrt{1+x^{-3}}}, \quad (110)$$

where $r^*(\kappa_i)$ is the solution of equation $\bar{\kappa}_i(r^*|r) = \kappa_i$.

Assuming now that time is large, we see from Eq. (109) that the maximum average in-degree scales at $r \gg 1$ as

$$\bar{\kappa}_i(0|r) = \frac{4\pi}{3} \int_0^r \zeta^3(x) \frac{x^2 dx}{\sqrt{1+x^{-3}}} \approx \frac{4\pi}{3} \zeta_\infty^3 \int_0^r x^2 dx = \frac{4\pi}{9} (\zeta_\infty r)^3, \quad \text{where} \quad (111)$$

$$\zeta_\infty = \zeta(\infty) = \int_0^\infty \frac{dx}{x^2 \sqrt{1+x^{-3}}} = \frac{2}{\sqrt{\pi}} \Gamma\left(\frac{1}{3}\right) \Gamma\left(\frac{7}{6}\right) \quad (112)$$

is the conformal time at the future infinity. Since r grows exponentially with time in this era, so does the average in-degree of the oldest nodes according to Eq. (111). In the long time limit, and for degrees well below the maximum average degree, $\kappa_i \ll \bar{\kappa}_i(0|r)$, we have $r > r' \gg 1$. Keeping the first two terms in the Taylor expansion of Eq. (108) for $r \gg 1$, we approximate conformal time by $\zeta(r) \approx \zeta_\infty - 1/r$. Inserting this approximation into Eqs. (109,110), and neglecting x^{-3} there, we obtain the implicit expression for the in-degree distribution at the future infinity,

$$Q(\kappa_i, \infty) = \frac{9}{4\pi} \frac{1}{x(\kappa_i)^3 [x(\kappa_i) - 1]^3}, \quad (113)$$

where $x(\kappa_i)$ is the solution of equation

$$\kappa_i = \frac{2\pi}{9} [(x-1)(2x^2 - 7x + 11) - 6 \ln x], \quad (114)$$

in the region $x \geq 1$. The last two equations give a nearly exact solution for the asymptotic in-degree distribution in a flat universe, because all the approximations that we have made so far become exact in the $t, r \rightarrow \infty$ limit. The only approximation that is not rigorously exact is the one due to the Laplace method in Section III B, yet given the astronomical value of node density δ in Eq. (57) used in this approximation, it can be also considered exact. We also note that the distribution is properly normalized since $\int_1^\infty Q(x, \infty) (\kappa_i)'_x dx = 1$.

Finally, we find approximations to this exact solution for small and large degrees. If $\kappa_i \ll 1$, then the solution of Eq. (114) scales as $x(\kappa_i) = 1 + (3\kappa_i/\pi)^{1/4}$, whereas for $\kappa_i \gg 1$, the scaling is $x(\kappa_i) = (9\kappa_i/4\pi)^{1/3}$. Substituting these scalings into Eq. (113), and neglecting insignificant terms there, we obtain

$$Q(\kappa_i, \infty) \approx \begin{cases} \frac{3}{4} \left(\frac{3}{\pi}\right)^{\frac{1}{4}} \kappa_i^{-\frac{3}{4}} & \text{if } \kappa_i \ll c, \\ \frac{4\pi}{9} \kappa_i^{-2} & \text{if } \kappa_i \gg c, \end{cases} \quad (115)$$

where the crossover degree value $c = 1.66$ is given by equating the two approximations above. Figure 10 shows the exact numerical solution for the in-degree distribution at $t = \infty$, and juxtaposes it against these two approximations. The match is remarkable.

We conclude that in-degree distribution in the universe causet at long times converges to the time-independent distribution, which is a power law with exponent $\gamma = 3/4$ for small degrees $k_i \in [1, c\delta a^4]$, whereas for large degrees $k_i > c\delta a^4$, it is a power law with exponent $\gamma = 2$.

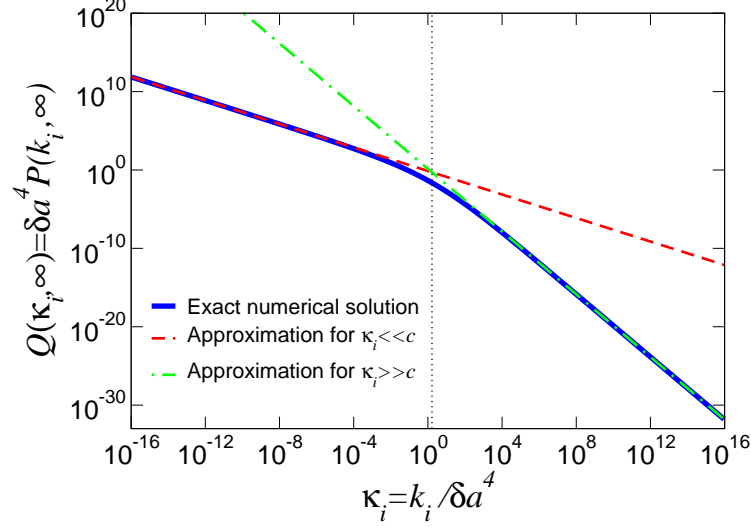


FIG. 10: Exact numerical solution versus approximations for the in-degree distribution in the universe causet at the future infinity. The solid line shows the numeric solution in Eqs. (113,114), while the dashed(-dotted) lines are the two approximations in Eq. (115) for $\kappa_i \ll c$ and $\kappa_i \gg c$. The crossover degree value c is shown by the dotted vertical line.

G. Numeric evaluation of the analytic solution

Given the results in the previous sections, the precise steps to numerically evaluate the analytic solution for the in-degree distribution in the universe at any given time are:

1. For a given rescaled age of the universe τ , e.g. $\tau = \tau_0$, compute the current value of the rescaled scale factor

$$r(\tau) = \sinh^{\frac{2}{3}} \frac{3}{2} \tau, \quad (116)$$

and the normalization factor

$$\mathcal{N}(\tau) = \frac{1}{6} (\sinh 3\tau - 3\tau). \quad (117)$$

2. According to Eq. (91), define function

$$\zeta(r) = 2\sqrt{r} {}_2F_1\left(\frac{1}{6}, \frac{1}{2}, \frac{7}{6}, -r^3\right), \quad (118)$$

where ${}_2F_1$ is the hypergeometric function.

3. Generate a (log-spaced) sequence of rescaled in-degrees κ_i , and for each value of κ_i in the sequence, find numerically the solution $r^*(\kappa_i) \in [0, r(\tau)]$ of equation

$$\kappa_i = \frac{4\pi}{3} \int_{r^*(\kappa_i)}^{r(\tau)} [\zeta(x) - \zeta(r^*(\kappa_i))]^3 \frac{x^2 dx}{\sqrt{1+x^{-3}}}. \quad (119)$$

4. With $r^*(\kappa_i)$ and $r(\tau)$ at hand, compute numerically the integral

$$\Phi(\kappa_i, r(\tau)) = 4\pi \int_{r^*(\kappa_i)}^{r(\tau)} [\zeta(x) - \zeta(r^*(\kappa_i))]^2 \frac{x^2 dx}{\sqrt{1+x^{-3}}}. \quad (120)$$

5. Finally, according to Eq. (70), the value of the rescaled in-degree distribution at κ_i is given by

$$Q(\kappa_i, \tau) = \frac{[r^*(\kappa_i)]^4}{\mathcal{N}(\tau)\Phi(\kappa_i, r(\tau))}. \quad (121)$$

H. Universality of $\gamma = 3/4$ scaling for small degrees

The portion of the degree distribution with exponent $\gamma = 3/4$ for small degrees below $\sim \delta a^4$ remaining in the universe causet even at long times may appear as a paradox at the first glance. Indeed, at long times, the universe is in its accelerating era dominated by dark energy, and the scale factor grows exponentially, versus polynomial growth in the matter-dominated era. Yet the degree distribution for small degrees behaves exactly the same way as in a matter-dominated universe, i.e. it has the same exponent $\gamma = 3/4$.

The intuitive explanation of this paradox is as follows [41]. The degree distribution in the range of small degrees is shaped by spacetime quanta born at times η' near the current time η . The future horizon radii of these nodes are smaller than the Hubble radius $1/H_0 \sim a$. Therefore these nodes do not yet “feel” the acceleration of the universe. For them the universe expands as if it was matter-dominated.

To formalize this intuition we check analytically that exponent $\gamma = 3/4$ for degrees $k_i \ll \delta a^4$ is universal for any scale factor. Keeping only the first term in the Taylor expansion of $\bar{k}_i(\eta'|\eta)$ at $\eta' = \eta$, we approximate

$$\bar{k}_i(\eta'|\eta) \approx \frac{1}{3}\pi\delta R^4(\eta)(\eta' - \eta)^4. \quad (122)$$

Using this approximation to solve equation $k_i = \bar{k}_i(\eta'|\eta)$ for $\eta^*(k_i)$, and substituting the solution into Eq. (70), we obtain

$$P(k_i, \eta) \approx \left(\frac{3}{\pi\delta}\right)^{1/4} \frac{R^3(\eta)}{4\mathcal{N}(\eta)} k_i^{-3/4}, \quad (123)$$

The degree distribution for small degrees is thus a power law with universal exponent $\gamma = 3/4$, while the scale factor is relegated to normalization. The scale factor is important only for old spacetime quanta with large degrees, where its exponential growth in asymptotically de Sitter spacetimes is responsible for the emergence of exponent $\gamma = 2$.

IV. RELATED WORK

The idea of replacing continuum spacetime with a graph or network appears in many approaches to quantum gravity, as it is a natural way to describe a discrete geometry. Causal Dynamical Triangulations (CDTs), for example, are formulated in terms of a simplicial triangulation of spacetime, which can be regarded as a (fixed valence) graph in which adjacent simplices are connected by an edge [42, 43]. Another popular approach to quantum gravity is Loop Quantum Gravity, where the quantum states of geometry are described naturally in terms of *spin networks*, which are graphs embedded into a three dimensional manifold. The edges and vertices in these graphs are colored with various mathematical structures, see [44] and references therein. There are a multitude of other approaches whose mathematical formulations have a similar discrete network-like character, such as Wolfram’s evolving networks [45], “quantum graphity” [46], D’Ariano’s causal networks [47], Requardt’s lumpy networks [48], etc.

Most descriptions of quantum spacetime geometry in terms of a graph structure are of a purely *spatial* character, in that the description of *spacetime* arises from some form of temporal evolution of the graph whose edges usually connect spatially nearest neighbors. The intuition behind this idea is clear, being similar to the idea of approximating a continuous space by a fine lattice embedded in it. However, the precise physical meaning of the “time” in which the network evolves, and the manner in which the Lorentz invariant nature of special relativity can emerge from such discreteness, are often unclear [11]. Causal sets and CDTs, however, are different in that they are described in terms of a graph-like structure which has a fundamentally *spacetime* character.

The degree of a node is an effective measure of its age in growing complex networks. This simple observation led us here to establishing a connection between these networks and the causal networks of discrete spacetime. As a final note, the notion of degree as a measure of time is reminiscent of unimodular gravity [49].

Acknowledgments

We thank M.Á. Serrano, M. Norman, J. Garriga, Z. Toroczkai, F. Papadopoulos, G. Bianconi, F. Bonahon, kc claffy, L. Klushin, S. Paston, and V.D. Lyakhovsky for useful discussions and suggestions. Special thanks to D. Chialvo for sharing his brain data with us. We also thank M. Norman for providing computing time at the SDSC through the director’s discretionary fund. This work was supported by NSF grants No. CNS-0964236 and CNS-1039646; Cisco Systems; Foundational Questions Institute grant No. FQXi-RFP3-1018; George W. and Carol A. Lattimer Campus Professorship at UCSD; MICINN project No. FIS2010-21781-C02-02; Generalitat de Catalunya grant No. 2009SGR838; and by the ICREA Academia prize 2010, funded by the Generalitat de Catalunya.

-
- [1] S. W. Hawking and G. F. R. Ellis, *The Large Scale Structure of Space-Time* (Cambridge University Press, Cambridge, 1975).
 - [2] F. Mattern, in *Proc Parallel and Distributed Algorithms*, edited by M. Corsnard et al. (Elsevier, Amsterdam, 1988), pp. 215–226.
 - [3] G. Korniss, M. A. Novotny, H. Guclu, Z. Toroczkai, and P. A. Rikvold, *Science* **299**, 677 (2003).
 - [4] L. J. Siegel, *Criminology* (Wadsworth Publishing, Belmont, 2011).
 - [5] R. Groff, ed., *Revitalizing Causality: Realism about Causality in Philosophy and Social Science* (Routledge, New York, 2008).
 - [6] L. Bombelli, J. Lee, D. Meyer, and R. Sorkin, *Phys Rev Lett* **59**, 521 (1987).
 - [7] D. B. Malament, *J Math Phys* **18**, 1399 (1977).
 - [8] S. W. Hawking, A. R. King, and P. J. McCarthy, *J Math Phys* **17**, 174 (1976).
 - [9] E. C. Zeeman, *J Math Phys* **5**, 490 (1964).
 - [10] C. Kiefer, *Quantum Gravity* (Oxford University Press, New York, 2007).
 - [11] L. Bombelli, J. Henson, and R. Sorkin, *Mod Phys Lett A* **24**, 2579 (2009).
 - [12] D. Rideout and R. Sorkin, *Phys Rev D* **61**, 024002 (1999).
 - [13] M. Ahmed and D. Rideout, *Phys Rev D* **81**, 083528 (2010).
 - [14] S. Perlmutter, G. Aldering, M. D. Valle, S. Deustua, R. S. Ellis, S. Fabbro, A. Fruchter, G. Goldhaber, D. E. Groom, I. M. Hook, et al., *Nature* **391**, 51 (1998).
 - [15] A. G. Riess, A. V. Filippenko, P. Challis, A. Clocchiatti, A. Diercks, P. M. Garnavich, R. L. Gilliland, C. J. Hogan, S. Jha, R. P. Kirshner, et al., *Astron J* **116**, 1009 (1998).
 - [16] J. B. Griffiths and J. Podolský, *Exact Space-Times in Einstein’s General Relativity* (Cambridge University Press, Cambridge, 2009).
 - [17] G. J. Galloway and D. A. Solis, *Classical Quant Grav* **24**, 3125 (2007).
 - [18] F. Papadopoulos, M. Kitsak, M. A. Serrano, M. Boguñá, and D. Krioukov, arXiv:1106.0286 (2011).

- [19] M. E. J. Newman, *SIAM Rev* **45**, 167 (2003).
- [20] S. Boccaletti, V. Latora, Y. Moreno, M. Chavez, and D.-U. Hwang, *Phys Rep* **424**, 175 (2006).
- [21] V. Eguíluz, D. Chialvo, G. Cecchi, M. Baliki, and A. V. Apkarian, *Phys Rev Lett* **94**, 018102 (2005).
- [22] K. Claffy, Y. Hyun, K. Keys, M. Fomenkov, and D. Krioukov, in *Proceedings of the 2009 Cybersecurity Applications & Technology Conference for Homeland Security (CATCH 2009), Washington, DC, March 3-4, 2009* (IEEE Computer Society, 2009), pp. 205–211, URL <http://www.caida.org/projects/ark/>.
- [23] J. Cannon, W. Floyd, R. Kenyon, and W. Parry, in *Flavors of Geometry*, edited by S. Levy (MSRI, Berkeley, 1997), pp. 59–116.
- [24] N. Arkani-Hamed, L. Hall, C. Kolda, and H. Murayama, *Phys Rev Lett* **85**, 4434 (2000).
- [25] R. Sorkin, A. Rajantie, C. Contaldi, P. Dauncey, and H. Stoica, in *AIP Conf Proc* (AIP, 2007), vol. 957, pp. 142–153.
- [26] J. Barrow and D. Shaw, *Phys Rev Lett* **106**, 101302 (2011).
- [27] D. Fraiman, P. Balenzuela, J. Foss, and D. Chialvo, *Phys Rev E* **79**, 061922 (2009).
- [28] G. Siganos, M. Faloutsos, P. Faloutsos, and C. Faloutsos, *IEEE ACM T Network* **11**, 514 (2003).
- [29] A. Dhamdhere and K. Dovrolis, in *Proceedings of the 8th ACM SIGCOMM Conference on Internet Measurement (IMC 2008), Vouliagmeni, Greece, October 20-22, 2008*, edited by K. Papagiannaki and Z.-L. Zhang (ACM, 2008), pp. 183–196.
- [30] B. Zhang, R. Liu, D. Massey, and L. Zhang, *Comput Commun Rev* **35**, 53 (2005).
- [31] P. Mahadevan, D. Krioukov, M. Fomenkov, B. Huffaker, X. Dimitropoulos, K. Claffy, and A. Vahdat, *Comput Commun Rev* **36**, 17 (2006).
- [32] M. Postnikov, *Geometry VI: Riemannian Geometry* (Springer-Verlag, Berlin, 2001).
- [33] F. Bonahon, *Low-Dimensional Geometry* (AMS, Providence, 2009).
- [34] D. Krioukov, F. Papadopoulos, M. Kitsak, A. Vahdat, and M. Boguñá, *Phys Rev E* **82**, 36106 (2010).
- [35] M. Kleban, *Class Quant Grav* **28**, 204008 (2011).
- [36] E. Komatsu, K. M. Smith, J. Dunkley, C. L. Bennett, B. Gold, G. Hinshaw, N. Jarosik, D. Larson, M. R.olta, L. Page, et al., *Astrophys J Suppl S* **192**, 18 (2011).
- [37] R. P. Woodard, *Rep Prog Phys* **72**, 126002 (2009).
- [38] M. Boguñá and R. Pastor-Satorras, *Phys Rev E* **68**, 36112 (2003).
- [39] D. Edwards, *Mon Not R Astr Soc* **159**, 51 (1972).
- [40] S. Weinberg, *Cosmology* (Oxford University Press, New York, 2008).
- [41] J. Garriga, *Private communications* (2012).
- [42] J. Ambjørn, J. Jurkiewicz, and R. Loll, *Phys Rev D* **72**, 064014 (2005).
- [43] J. Ambjørn, J. Jurkiewicz, and R. Loll, *Sci Am* pp. 42–49 (2008).
- [44] C. Rovelli and S. Speziale, *Phys Rev D* **82**, 44018 (2010).
- [45] S. Wolfram, *A New Kind of Science* (Wolfram Media, Champaign, IL, 2002).
- [46] T. Konopka, F. Markopoulou, and S. Severini, *Phys Rev D* **77**, 104029 (2008).
- [47] G. M. D’Ariano and A. Tosini, arXiv:1109.0118 (2011).
- [48] M. Requardt, arXiv:gr-qc/0308089 (2003).
- [49] A. Daughton, J. Louko, and R. Sorkin, in *Proceedings of the 5th Canadian Conference on General Relativity and Relativistic Astrophysics, University of Waterloo, 13-15 May, 1993*, edited by R. B. Mann and R. G. McLenaghan (World Scientific, Singapore, 1994), pp. 181–185.